Forschungszentrum Karlsruhe
Technik und Umwelt

Wissenschaftliche Berichte
FZKA 5860

Numerical Modeling of the Influence of non-LTE Effects on the MIPAS Balloon and Satellite Limb Radiance Measurements

V. S. Kostsov, H. Fischer, Yu. M. Timofeyev, H. Oelhaf

Institut für Meteorologie und Klimaforschung

Dezember 1996

Forschungszentrum Karlsruhe
Technik und Umwelt
Wissenschaftliche Berichte
FZKA 5860

Numerical Modeling of the Influence of non-LTE Effects on the MIPAS Balloon and Satellite Limb Radiance Measurements

V.S. Kostsov*, H. Fischer, Yu.M. Timofeyev*, H. Oelhaf

Institut für Meteorologie und Klimaforschung

*Research Institute of Physics, St. Petersburg State University, Russia

Forschungszentrum Karlsruhe GmbH, Karlsruhe
1996

Forschungszentrum Karlsruhe GmbH
Postfach 3640, 76021 Karlsruhe

ISSN 0947-8620

Abriß

Numerische Modellierung des Einflusses des nicht vorhandenen lokalen thermodynamischen Gleichgewichts (non-LTE) auf MIPAS Ballon- und Satelliten-Horizontsondierungsmessungen

Dieser Bericht enthält die Ergebnisse von Untersuchungen, die im Rahmen eines Kooperationsvertrags für den Zeitraum von 1993 bis 1995 zwischen dem Institut für Meteorologie und Klimaforschung, Forschungszentrum Karlsruhe und dem Forschungsinstitut für Physik der Staatsuniversität St.Petersburg, Rußland durchgeführt wurden.

Verschiedene Atmosphärenmodelle und Computerprogramme, die die Besetzung von Schwingungszuständen von Molekülen atmosphärischer Gase bei nicht-lokalem thermodynamischem Gleichgewicht (non-LTE) beschreiben und atmosphärische Strahldichten bei non-LTE Bedingungen simulieren, wurden berücksichtigt. Die Untersuchungen konzentrierten sich auf die Infrarotemissionen von Kohlendioxid und Ozon, die vom MIPAS-B Balloninstrument gemessen wurden, und in Zukunft auch vom MIPAS Satelliteninstrument während der Mission der Europäischen Polaren Plattform gemessen werden. Die non-LTE Emissionen von Stickstoffmonoxid wurden ebenfalls berücksichtigt. Basierend auf den verfügbaren non-LTE Modellen und Programmen wurde der Einfluß des non-LTE Effekts auf die MIPAS Ballon- und Satellitenmessungen untersucht, zunächst hinsichtlich der Nachweisbarkeit des Effekts, und später auch bezüglich der Ableitung von Vertikalverteilungen der Temperatur und Spurengase.

Die Analyse der MIPAS-B Messungen des Ballonfluges 1990 zeigte, daß der non-LTE Effekt bei diesem Flug nicht nachgewiesen werden konnte, und zwar aufgrund des im Vergleich zum spektralen Rauschen (NESR) geringen non-LTE Beitrags zur Strahldichte im Spektralintervall 930-990 cm^{-1}. Die Simulation von ballongestützten Horizontsondierungsmessungen im Spektralinterval 990-1030 cm^{-1}, das im Bereich des Zentrums der 9.6 μm Ozon-Bande liegt, zeigte die Möglichkeit der Beobachtung des non-LTE Effekts, falls das spektrale Rauschen (NESR) kleiner oder gleich 0.2 $mW/(m^2\ sr\ cm^{-1})$ ist. In diesem Fall würde der non-LTE Effekt das Rauschen um einen Faktor 3 übertreffen.

Die Simulationen von Strahldichteprofilen und Spektren für die Horizontsondierungsgeometrie von einer Satellitenplattform wurden in den Spektralbereichen der 15 μm und 10 μm CO_2 Banden, der 9.6 μm O_3 Bande und der 5.3 μm NO Bande, die alle stark von non-LTE Effekten beeinflußt sind, durchgeführt. Ausgehend vom Vergleich der NESR des MIPAS

Satelliteninstrumentes und der non-LTE Beiträge zur spektralen Strahldichte wurden die Tangentenhöhenbereiche identifiziert, in denen der non-LTE Effekt von Bedeutung ist. Für CO_2 und O_3 wurden die Untersuchungen auf den Spektralbereich beschränkt, in dem zuvor Spektralintervalle ("Microwindows") für die Ableitung von Druck und Temperatur bestimmt worden waren. Die numerischen Simulationen zeigten, daß der non-LTE Einfluß auf die Strahldichte für die meisten Microwindows vernachläßigbar klein ist, mit Ausnahme jener, die CO_2 Linien der sogenannten 10 μm Laser-Bande enthalten. Die Erhöhung der Strahldichte in den Zentren dieser Linien aufgrund des non-LTE Effekts kann das Rauschen der MIPAS Messungen im Tangentenhöhenbereich von 30 bis 80 km beträchtlich überschreiten. Falls diese Microwindows für die Bestimmung von Druck und Temperatur verwendet werden, ist es notwendig, den non-LTE Effekt geeignet zu berücksichtigen. Die numerischen Simulationen der non-LTE Emissionen von NO zeigten die Notwendigkeit der Berücksichtigung des non-LTE Effekts für die NO Schwingungsfundamentalbande bei der Interpretation der MIPAS Horizontsondierungsmessungen in Tangentenhöhen oberhalb von 50 km.

Das Problem der Druck-Temperatur Profil-Bestimmungen aus den MIPAS Messungen in den vorausgewählten Microwindows im Spektralbereich von 10 bis 15 μm wurde auf der Basis numerischer Simulationen untersucht. Die Profile von Druck und Temperatur wurden mit Hilfe eines Mehr-Parameter "General Optimal Estimation"-Algorithmus unter Berücksichtigung des non-LTE Effekts und verschiedener Annahmen und a priori Informationen über den Zustand der Atmosphäre abgeleitet. Basierend auf den Fehler-Matrix Rechnungen und simulierten Retrievals können die folgenden Schlussfolgerungen gezogen werden: (1) Der Einfluß von non-LTE Effekten auf die Retrievals ist vernachläßigbar klein, wenn die verwendeten Microwindows keine CO_2 Laserlinien enthalten; (2) Die Unsicherheiten der Ozon Teilchenzahldichte kann die Ergebnisse der Druck-Temperatur Retrievals beträchtlich stören, falls sie nicht berücksichtigt werden. Aus diesem Grund sollten die Spektralbereiche für die Druck-Temperaturbestimmung auf die der vorausgewählten "Microwindows" beschränkt werden, die hinreichend frei von Ozon-Signaturen sind.

Empfehlungen für weitere Untersuchungen des non-LTE Effekts im Hinblick auf die geplanten satellitengetragenen MIPAS Messungen wurden ausgearbeitet.

Abstract

Numerical Modeling of the Influence of non-LTE Effects on the MIPAS Balloon and Satellite Limb Radiance Measurements

The report contains the results of investigations performed in frame of Cooperation Agreement for 1993-1995 between the Institut für Meteorologie und Klimaforschung, Forschungszentrum Karlsruhe, and the Research Institute of Physics at St.Petersburg State University, Russia.

Several atmospheric models and computer codes, which describe the non-LTE (non-local thermodynamic equilibrium) populations of vibrational states of molecules of atmospheric gases and simulate non-LTE atmospheric radiance, have been considered. The particular attention has been paid to infrared emissions by carbon dioxide, ozone, which have been measured by the MIPAS-B instrument (balloon flights) and will be measured by the MIPAS instrument during the future European Polar Platform space mission. Nitric oxide non-LTE emissions have been considered also. On the basis of the available non-LTE models and codes the influence of the non-LTE effect on the MIPAS balloon-borne and space-borne measurements has been studied, first, from the point of the detectability of the effect, and, second, regarding the retrieval of the vertical distributions of temperature and gas composition.

The analysis of the MIPAS-B 1990 balloon campaign data have shown that the non-LTE effect could not be detected in this campaign due to the small values of the non-LTE contribution to radiance in the spectral range of measurements (930-990 cm^{-1}) if compared to the noise equivalent spectral radiance (NESR). The simulation of the balloon-borne limb radiance measurements in the interval 990-1030 cm^{-1}, which is close to the center of the ozone 9.6 μm band, has shown the possibility to detect the non-LTE effect if NESR is equal or better than 0.2 $mW/(m^2 sr\ cm^{-1})$. In this case the non-LTE effect will exceed the NESR by a factor of 3.

The simulations of limb radiance profiles and spectra for the limb viewing geometry and space-borne platforms have been performed in the spectral regions of 15 μm and 10 μm CO_2, 9.6 μm O_3 and 5.3 μm NO absorption bands which are strongly influenced by the non-LTE effect. On the basis of the comparison of NESR of MIPAS and the non-LTE contribution to radiance, the tangent height ranges, where this contribution is considerable, have been identified. For CO_2 and O_3, the analysis has been limited to the spectral region where the set of microwindows preselected for the pressure-temperature retrievals had been determined. The numerical simulations have shown that the influence of the non-LTE effect on limb radiance is negligibly

small in most of the microwindows except ones which contain CO_2 lines of the so-called 10 μm laser transition. The enhancement of radiance in the centers of these lines due to the non-LTE can exceed considerably the NESR of the MIPAS measurements for the tangent heights of observations in the range of 30-80 km. Therefore, if corresponding microwindows are used for the pressure-temperature retrievals, it is necessary to account for non-LTE effect in a suitable way. The numerical simulations of the non-LTE emission from NO have shown the necessity to account for non-LTE effect for the NO fundamental vibrational transition while interpreting the MIPAS limb measurements for the tangent heights up to 50 km.

The problem of the pressure-temperature retrievals from the MIPAS measurements in the area of preselected microwindows (spectral region 10-15 μm) has been investigated on the basis of numerical experiments. The model pressure and temperature profiles have been retrieved by the multi-parameter general optimal estimation algorithm accounting for the non-LTE effect and using different assumptions and a priori information on the atmospheric state. On the basis of the error matrix calculations and simulated retrievals, the following main conclusions can be stated: (1) the influence of non-LTE effect on the results of the retrieval is negligibly small if the set of microwindows does not include the CO_2 "laser" lines; (2) the uncertainties of ozone number density can considerably distort the results of the pressure-temperature retrievals if not taken into account. Therefore the spectral regions for the p-T retrieval should be limited to the preselected microwindows which are sufficiently free of ozone signatures.

Recommendations for further investigations of the non-LTE effect with respect to the planned MIPAS space-borne measurements have been worked out.

TABLE OF CONTENTS

1. Introduction.

The progress of experimental techniques made it possible during the last years to develop the instruments for high-resolution and high-precision measurements of atmospheric infrared emissions. MIPAS (Michelson Interferometer for Passive Atmospheric Sounding) is one of such instruments, which will be part of the core payload for the European Polar Platform and is to be launched in 1999. It is designed to obtain high-resolution (0.05 cm^{-1}) limb radiance spectra in broad spectral intervals (4-15 μm) for tangent heights from 5 km up to 150 km. On the basis of the MIPAS measurements it is planned to solve a number of inverse problems of the remote sensing of the atmospheric temperature distribution and gaseous composition. In order to obtain the highest possible accuracy of the retrieval of the vertical profiles of temperature and atmospheric species it is necessary to account for all effects which can have an influence on the radiative transfer process, for example the departure from local thermodynamic equilibrium (LTE). Accounting for non-LTE is of particular importance for the scenario of the experiment which includes measurements of the emissions from upper atmospheric layers, where this effect is the most pronounced. From the other point, besides the retrieval of the temperature profiles and gas composition (when the non-LTE effect is considered as an "interfering" one), the investigation of the non-LTE effect itself on the basis of the MIPAS measurements is a very important task.

The term "departure from the local thermodynamic equilibrium" or "non-LTE effect" refers to the situation when the distribution of populations of states of molecules deviates from the Boltzmann's law. Such situation is stipulated by thermal and different non-thermal processes in the atmospheric layers where the molecular collisions no longer play the dominant role in maintaining the population of the states. The non-LTE effect can influence the vibrational levels of molecules and the rotational ones as well. However, for many atmospheric situations the ratio of rotational populations is still maintained under LTE while there is a breakdown of LTE for the vibrational populations. Such situation is rather common in the atmosphere up to the altitudes of 100-120 km and is called "vibrational non-LTE". Below we shall consider this case omitting the word "vibrational".

The non-equilibrium population of the i-th vibrational level of a molecule is usually expressed in terms of vibrational temperature T_v, defined as follows:

$$T_v = \frac{E_v}{k \ \ln(n_0 g_v / n_v)} \qquad \textbf{(Eq. 1.1)}$$

where k is Boltzmann constant, E_v is the energy of the vibrational level v, g_v is the statistical weight factor, n_v is the population of the level, and n_0 is the concentration of molecules. Under this definition T_v is referred to the total concentration of molecules (otherwise the vibrational temperature may be referred to a specific transition between two levels).

The altitude levels of the breakdown of LTE conditions (i.e. the levels where T_v starts to deviate from the kinetic temperature T_{kin}) are different for different gases and their absorption bands. For a specific problem of the atmospheric remote sensing which is to be solved, it is necessary to consider a combination of factors while studying the influence of the non-LTE effect on the results of the remote sensing. These factors are:

- spectral range of measurements and, hence, "optically active" atmospheric species which display non-LTE features and have absorption bands falling in the measurement spectral channels;

- atmospheric conditions which influence the process of radiative transfer itself and the processes of excitation and deexcitation of molecules of gases under non-LTE;
- spectral resolution of an instrument;
- noise level of an instrument (noise equivalent spectral radiance - NESR).

A number of atmospheric gases (CO_2, O_3, H_2O, CO, NO, NO_2) exhibit non-LTE features which influence their emissions in the infrared region, where the MIPAS measurement channels are located (see **Table 1.1**). We stress that in the frame of the preparations for the space mission, the characteristics of the MIPAS instrument are permanently improved, so the data presented in the table may change, though the principal locations of the channels remain practically the same. One of the most important are CO_2 15 μm and 10 μm bands, O_3 9.6 μm band and NO 5.3 μm bands which fall into the channels 1, 2, 4, and 5. Therefore, there is a necessity to investigate a possible influence of the non-LTE effect on the results of the MIPAS measurements, first of all simulating the detected atmospheric radiance accounting for non-LTE. In case this influence is considerable (i.e. the non-LTE emission contribution is comparable with NESR), the second step should be devoted to the solution of the problem of the development of special algorithms accounting for this effect while processing measurement data and solving different inverse problems of remote sensing.

Table 1.1 The MIPAS measurement channels.

Channel number	Wavenumber interval [cm^{-1}]	NESR [$mW/(m^2\ sr\ cm^{-1})$]
1	685 - 970	0.35
2	1020 - 1170	0.23
3	1215 - 1500	0.10
4	1570 - 1750	0.03
5	1820 -2410	0.03 - 0.02

The non-LTE effect has been studied theoretically and detected in the experiments for a large number of atmospheric gases (the overview of the relevant papers is given in the section "Atmospheric models, details of calculations"). The present study mainly deals with the consideration of the non-LTE effect in several absorption bands of CO_2, O_3 and NO. The problem of the non-LTE effect in the absorption bands of NO_2 is discussed in general.

Recently, a certain attention was paid to the development of different algorithms accounting for the non-LTE effect in the remote sensing problems. *Dem'yanikov and Kutepov* [1987, 1988] investigated a number of formulations of the solution of the remote sensing problem under conditions of LTE breakdown in the 15 μm CO_2 band for the limb radiance measurements with moderate resolution. *Oelhaf and Fischer* [1989] described the model for the investigation of non-LTE effect relevant to limb emissions of atmospheric constituents. In the paper by *Kutepov et al.* [1993] the effects of vibrational as well as rotational non-LTE of CO molecules on limb radiance distribution in the 4.7 μm band were analyzed and subsequent implications for remote sensing with high spectral resolution instruments were outlined. *Kostsov et al.* [1992a] studied the possibility of retrieving information on the vertical distributions of the vibrational temperatures for CO_2 from limb radiance measurements in the 15 μm absorption band and estimated the optimal spectral resolution for solving this problem on the basis of the analysis of the numerical simulations of non-LTE limb spectra. In the subsequent paper [*Kostsov et al.*, 1992b], the practical possibilities for solving the inverse problem of retrieval of the vibrational temperature profiles for the low-lying CO_2 vibrational states were investigated by numerical modeling of satellite measurements of limb radiance in the 15 μm band. The estimates of the retrieval accuracy were made for a MIPAS type apparatus. *Lopez-Puertas et al.* [1992] analyzed the upper atmospheric $CO_2(\nu_2)$ vibrational temperatures retrieved from ATMOS experiment Spacelab 3 spectra by using a non-LTE radiative transfer model. The general optimal estimation

technique was applied by *Kostsov et al.* [1995] and *Timofeyev et al.* [1995] to the problem of multi-parameter joint retrieval of vibrational temperatures, gas composition and kinetic temperature profiles. *Kostsov et al.* [1995] and *Timofeyev et al.* [1995] performed the numerical estimations of the retrieval accuracy for the simulated measurements by CLAES and MIPAS instruments in the 15 μm CO_2 bands, 9.6 μm O_3 bands and 10 μm CO_2 laser bands. *Ishov et al.* [1995] studied the possibility of the retrieval of the non-LTE ro-vibrational populations of the CO_2 molecules and line source functions from numerically simulated high resolution limb spectra in the 15 μm and 4.3 μm spectral regions, which imitate the limb radiance measurements to be obtained by MIPAS. The obtained quantities were used for the retrieval of kinetic and vibrational temperatures in the middle and upper atmosphere.

The preparation to the processing of the MIPAS data during the European Polar Platform mission stipulates the necessity to perform further investigations of the non-LTE effect in connection with the development of the efficient and rigorous retrieval algorithms. Therefore, in the present study the following topics were considered:

1. **"Forward" problem:** On the basis of the available data on the non-equilibrium populations of the vibrational states of molecules of several atmospheric gases the possible influence of the non-LTE effect on the MIPAS balloon-borne and space-borne measurements was studied. The 15 μm CO_2 bands, 9.6 μm O_3 bands, 10 μm CO_2 laser bands and 5.3 μm NO bands were considered. The simulated atmospheric limb radiances were compared to the values of NESR and the conclusions were made on the altitude range and the magnitude of the non-LTE contribution to the measured radiances.

2. **Inverse problem:** The general optimal estimation algorithm accounting for non-LTE was applied to the investigation of the accuracy of the joint pressure-temperature retrieval from the measurements in the 15 μm band spectral region, where the microwindows, preselected for p-T retrieval by *Clarmann et al.* [1994] are located. (These microwindows were improved in further studies.) The space-borne remote sensing experiment was numerically simulated and the model pressure and temperature profiles were retrieved using different assumptions on the atmospheric state. On the basis of the accuracy estimations, the conclusions were done on the influence of non-LTE effect and the uncertainties of ozone number density on the pressure-temperature retrieval accuracy.

2. Atmospheric models.

The non-LTE atmospheric model suitable for the limb radiance simulations should comprise the set of vertical profiles including: pressure, kinetic temperature, number densities of the optically active gases, and the vibrational temperatures of the vibrational states which are involved in the transitions falling in the considered spectral interval. The model should be self consistent, i.e. all profiles should correspond to the same atmospheric conditions (time, season, geographic region). In reality, the development of such complete and self consistent non-LTE models is very problematic due to the complexity of the problem of calculation of the non-LTE populations. The solution of this problem even for a rather limited number of species (one-two) involves modeling of many processes and also requires a number of certain assumptions and simplifications. Currently, we have no information on the complete non-LTE model which describes the non-LTE features of several atmospheric gases simultaneously and is self consistent. Therefore, in our limb radiance simulations we used models which were compiled on the basis of separate non-LTE models developed for specific atmospheric gases.

Carbon dioxide is the atmospheric component, for which the non-LTE effect was studied in great detail. In the papers by *Kutepov and Shved*, [1978], *Lopez-Puertas et al.* [1986a,b], the deviation from LTE was considered for the vibrational levels which are associated with the 15 μm and 4.3 μm CO_2 absorption bands. The vibrational temperature profiles and the values of cooling rates were estimated for different atmospheric conditions in the altitude range from 40 up to 120-140 km. In the paper by *Lopez-Puertas and Taylor* [1989], the populations of the vibrational levels have been evaluated accounting for diurnal, latitudinal and seasonal variations and the non-LTE model has been validated using the data from SAMS. In the above mentioned papers the radiative excitation was treated by Curtis matrix method. Line-by-line algorithm for the radiative excitation was applied by *Wintersteiner et al.* [1992], who calculated the vibrational temperatures for CO_2 levels, cooling rates and limb radiances in the altitude range 50-140(180) km and validated the non-LTE model using the experimental data from SPIRE. In the work by *Ogibalov et al.* [1995], the line-by-line ALI (accelerated lambda iteration) technique was applied to the solution of the radiative transfer problem for a great number of the CO_2 bands. This model embraces for day and night conditions 334 vibrational levels of 8 carbon dioxide isotopes that give rise to 784 bands (with 103000 ro-vibrational lines) in the 1-15 μm region.

The non-LTE features of ozone molecules have been studied also in detail. *Green et al.* [1986] derived the populations of ozone vibrational states in the altitude range 70-100 km from the limb radiance measurements obtained in the SPIRE experiment. *Mlynczak and Drayson* [1990a,b] developed two statistical equilibrium models for ozone and investigated the non-LTE effect in the altitude range 0-115 km. *Manuilova and Shved* [1992] developed the non-LTE model for ozone which comprehends a large number of vibrational levels. This model was used for the simulations of the non-LTE population distributions and non-LTE atmospheric radiances originated from different ozone bands accounting for different atmospheric conditions and different processes of excitation and deexcitation. The estimated values of non-LTE radiance in ozone bands were also reported by *Fichet et al.* [1992].

In the study of the influence of the non-LTE effect on limb radiance in the 10-15 μm region we used the non-LTE model comprising two gases under non-LTE (CO_2 and O_3). H_2O was considered under LTE conditions. The vibrational temperature profiles for the states responsible for the 15 μm transitions were provided at our disposal by A.A.Kutepov. These profiles were generated on the basis of the algorithm described in the paper by *Kutepov and Shved* [1978], which was upgraded and included up-to-date values of the rate coefficients of different processes leading to non-LTE. The model included T_v for 7 lower vibrational states of the CO_2(626) molecule and T_v for the state 01101 of the (636), (628), and (627) CO_2 molecules. The non-LTE model for the 10 μm CO_2 band was available from M.Lopez-Puertas [*Lopez-*

Puertas, 1986a,b]. The model contains the vibrational temperature of the state 00011 of the main CO_2 isotope. The vibrational temperatures for CO_2 states are shown in **Figure 2.1**. It can be seen that the vibrational temperatures of all considered states except 00011 start to deviate from the kinetic temperature at the height of 70-90 km. For the state 00011 the departure from LTE starts already at about 60 km and the deviation from the kinetic temperature can reach 100 K near the mesopause.

The non-LTE model for ozone was based on the numerous calculations of vibrational temperature profiles for different atmospheric situations performed by *Manuilova and Shved* [1992]. We had at our disposal about 30 atmospheric models which describe both day-time and night-time non-LTE conditions for the 9.6 μm ozone band. In the present study we have used one of day-time models referred below as "moderate" because of the following reasons:

- the non-LTE effects are much stronger in the day-time;
- the chosen model describes the average values of physical parameters rather then exotic and therefore is more suitable for the purpose of estimations.

As an example, **Figure 2.2** presents the vibrational temperature profiles for ozone states corresponding to the chosen "moderate" model. We would like to draw attention to the large values of the vibrational temperatures, especially for upper levels. We stress, that for the case of the "extreme" non-LTE conditions these values are even higher, as reported by *Manuilova and Shved* [1992].

The kinetic temperature profile in the calculations performed by *Manuilova and Shved* [1992] corresponded to CIRA-72 model. The vibrational temperature profiles for all CO_2 states except

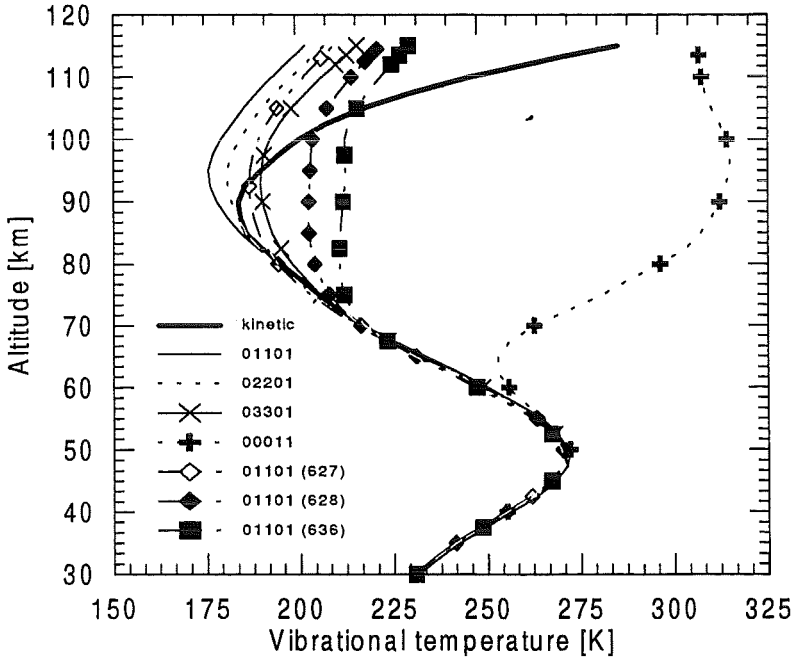

Fig. 2.1 Vibrational temperatures T_v for CO_2 lower vibrational states (see the legend) used in the non-LTE atmospheric model. The model is assumed to describe day-time conditions. Kinetic temperature is shown for the purpose of comparison. (Data source: A.A.Kutepov, M.Lopez-Puertas, private communication.)

00011 were generated also for the T_{kin} from CIRA-72. Since the T_v profile for the CO_2 state 00011 was generated for the US Standard 1976 model, we slightly adjusted it in order to match the CIRA-72 kinetic temperature profile in the atmospheric layers where the conditions of LTE are valid.

The profile of ozone number density was taken from *Manuilova and Shved* [1992] in order to keep self-consistency of the non-LTE model. Since the variations of CO_2 volume mixing ratio are negligibly small in the entire mesosphere, we took for all calculations the CO_2 profile from the AFGL-86 atmospheric model [*Anderson et al.*, 1986]. The water vapor profile has been taken also from [*Anderson et al.*, 1986].

The description and detailed discussions of the processes leading to the breakdown of LTE for the vibrational levels of carbon dioxide and ozone molecules can be found in the papers mentioned above in this section. Since the investigations of the non-LTE effect for NO and NO_2 are not so numerous, below we present a brief overview of this topic.

Degges [1971] predicted the non-LTE effects for NO (v=1,2) in the mesosphere and lower thermosphere, indicating that these states are populated through the following mechanisms:

- the transfer of vibrational quanta in collisions with molecular oxygen and nitrogen;
- atom exchange with atomic oxygen;
- absorption of infrared radiation from the earth's surface, the lower atmosphere and the sun;
- fluorescent decay of the β– , γ-, and δ-band systems following resonance absorption of solar ultraviolet radiation;
- electronic impact excitation;
- excitation during chemical formation.

These excitation mechanisms are balanced by collisional deexcitation and by radiation in the infrared vibration rotation bands. *Degges* [1971] estimated the relative importance of each of

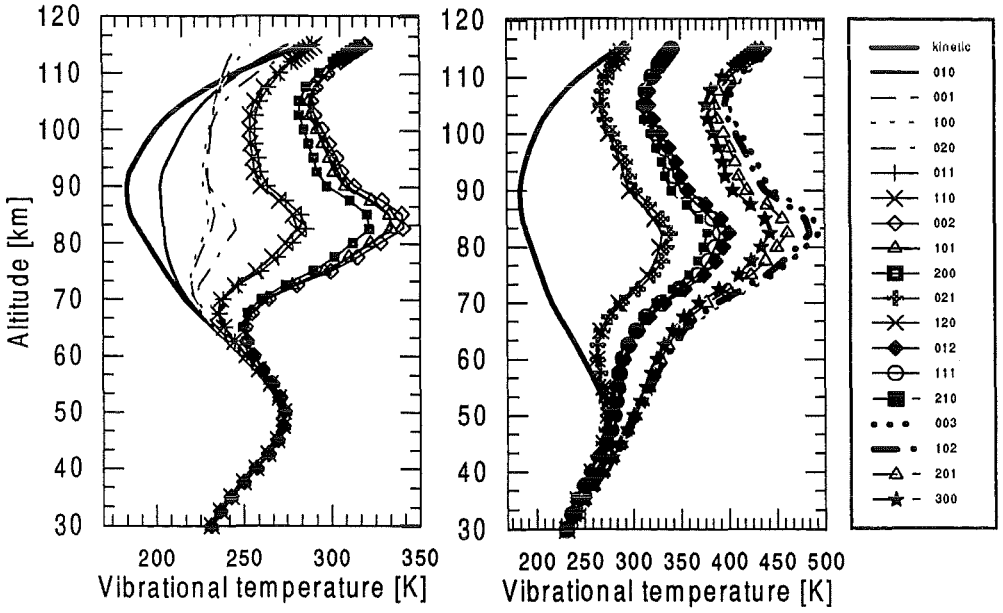

Fig. 2.2 Vibrational temperatures T_v for O_3 lower vibrational states (see the legend) used in the non-LTE atmospheric model. The model is assumed to describe day-time conditions and "moderate" non-LTE effect. Kinetic temperature is shown for the purpose of comparison. (Data source: R.O.Manuilova, private communication.)

these processes and indicated that between about 60 and 100 km the nitric oxide vibrational temperature is determined almost entirely by absorption and re-emission of surface, atmospheric, and solar radiation. The refined calculations of the magnitude of the non-LTE effects were performed by *Caledonia and Kennealy* [1982].

Nitric oxide is an important atmospheric component, it is a member of NO_y family and a major contributor to radiative cooling of the lower thermosphere. A simple formulation of the nitric oxide cooling by the emission of the 5.3 μm fundamental band in the terrestrial atmosphere was done by *Kockarts* [1980]. It was indicated that the cooling effect is highly variable as a consequence of its strong temperature dependence and of the observed variability of the nitric oxide concentration. *Kockarts* [1980] also reported that infrared emission from NO is never in local thermodynamic equilibrium above 120 km altitude and the predominant cooling probably occurs during NO auroral enhancements.

Kaye and Kumer [1987] have shown that the vibrational state populations of nitric oxide could be substantially different from that expected on the basis of local thermodynamic equilibrium throughout the stratosphere. Despite the fact that collisional quenching is rather fast for altitudes less than 50 km, the excitation of NO (v>0) due to photochemical processes is rapid enough that the stratospheric v>0 populations are significantly larger than would be predicted by LTE and this effect is greatly enhanced for NO (v>0) states. The vibrationally excited NO is produced in the reactions:

$$NO_2 + h\nu \rightarrow NO(v) + O$$
$$O + NO_2 \rightarrow NO(v) + O_2$$

Other processes which could contribute to non-LTE effects of stratospheric NO are the excitation of NO by absorption of upwelling earthshine and direct solar excitation of the 5.3 μm lines. However, the radiative excitation processes are relatively unimportant below 50 km altitude. *Kaye and Kumer* [1987] predicted the vibrational state distributions of newly formed NO as a function of altitude. They also presented the data which can be applied for calculation of vibrational temperature profile of the state v=1 in the altitude region 15-50 km.

There have been numerous observations of thermospheric NO emissions. The results of the most recent observations, which lead to the evidence of the non-LTE effects are briefly summarized below.

The ISAMS instrument on the UARS has made global measurements of emission from the 1→0 band of nitric oxide, using a limb viewing geometry in which the tangent point is scanned from 0 km to >150 km. Vertical profiles of atmospheric radiance often showed a peak around 120 km altitude, due to the relatively high temperatures and densities of NO (v=1) found in the lower thermosphere [*Ballard et al.*, 1993]. The data showed that the lower thermosphere is often the region from which most NO (1→0) emission originates, and that this emission is usually largest at high latitudes and is usually very variable, but there are periods where the emission is extremely disturbed and appears to be largest at mid- to equatorial latitudes. *Ballard et al.* [1993] indicated the probability, that the radiance enhancement at low latitudes was the result of simultaneous changes in T_{kin}, NO number density and the NO(v=1) source function as a result of particle precipitation. An increase in T_{kin} alone would require T_{kin}>700 K, while an increase in NO number density alone would require the path to become very opaque to NO(v=1) radiation. The source function was likely to be very different from that assumed at quiet times, due to changes in the chemical production of vibrationally excited NO. Therefore the radiance enhancement seemed to be an evidence of the considerable non-LTE effect. However, the ISAMS pressure modulated radiometer channel data alone gave no separate information about any enhancements to temperature or to the source function (i.e. to the population of the v=1 level).

The evidence of the non-LTE effects in the rotational structure of NO vibrational bands was reported by *Smith and Ahmadjian* [1993]. Band head emissions from highly rotationally excited NO(v,J) have been observed in the quiscent atmosphere at tangent heights between approximately 115 and 190 km for both sunlit and nighttime conditions. The data were obtained by the cryogenic CIRRIS-1A interferometer which was operated on board the space shuttle between 28 and 30 April 1991. The spectra were obtained with moderate (1.04 cm^{-1}) and low resolution (7.36 cm^{-1}). These observations were the first ones of very high, non-equilibrium rotational excitation of NO in the quiscent airglow.

As far as the non-LTE effect for NO_2 is concerned, it should be mentioned, that the evidence for nonlocal thermodynamic equilibrium in the ν_3 mode of stratospheric nitrogen dioxide was described by *Kerridge and Remsberg* [1989]. The LIMS instrument on Nimbus 7 measured H_2O and NO_2 emissions. There were 3 anomalous features observed: the daytime enhancement of H_2O, the high concentration of H_2O sometimes observed in the polar night mesosphere, and the high ratio of daytime/nighttime NO_2 in the upper stratosphere. These features were attributed to the departure from LTE of daytime emission, in particular, the high vibrational states of $NO_2(\nu_3)$ are pumped by absorption of visible and near-IR sunlight and by chemical reaction

$$NO + O_3 \rightarrow NO_2 + O_2$$

Kerridge and Remsberg [1989] have emphasized that in order for NO_2 hot bands to make a significant contribution to radiance, it is necessary for the populations of emitting states between v=2 and 9 to be greatly enhanced over LTE values. At the time of performing the current study, we had no non-LTE model for NO_2 at our disposal, therefore we did not perform numeric simulations of the non-LTE emissions from NO_2.

A large amount of data on the vibrational temperatures for several atmospheric species (H_2O, CO_2, O_3, CO and NO) is included in the line-by-line code for atmospheric transmittance and radiance calculations FASCOD3P. In particular, there are vibrational temperature profiles for the states of the NO molecule X1/2-1 and X1/2-2. These profiles, which we taken for the atmospheric limb emission simulations in the region of NO 5.3 μm bands, are shown in **Figure 2.3**. It should be mentioned, that NO has two vibrational manifolds emitting in the 5.3 μm region due to the splitting of the electronic state. Below we shall indicate every level explicitly (e.g. X1/2-1, X3/2-1, X1/2-2, X3/2-2, etc.). According to FASCOD3P dataset, the deviation from the local thermodynamic equilibrium starts already from the upper troposphere for the state X1/2-1 and the state X1/2-2 seems never to be in LTE. The vibrational temperature profiles have very small gradients, for example T_v of the state X1/2-2 is constant from 18 to 67 km and equal to 320 K. The deviations of the vibrational temperature profiles from the kinetic temperature profile have two maximums: one in the stratosphere and another in the vicinity of the mesopause. For the state X1/2-1 these deviations reach 30-40 K, and for the state X1/2-2 they can reach 100 K in the stratosphere and 150 K in the vicinity of the mesopause.

Figure 2.3 also shows the vibrational temperature profile for the state X1/2-1 which was calculated on the basis of data reported by *Kaye and Kumer* [1987] in the altitude range 15-50 km. *Kaye and Kumer* [1987] modeled the pumping of the first vibrational state by photochemical mechanism and presented the corresponding parameter and the relationship between this parameter and the vibrational temperature. As it can be seen from **Figure 2.3**, T_v(X1/2-1) calculated on the basis of data which were reported by *Kaye and Kumer* [1987] differs markedly from T_v which was taken from FASCOD3P dataset. The discrepancies could be explained by the different setting of a priori conditions for generating vibrational temperatures. However since there is no information on the initial conditions used for generation of the FASCOD3P vibrational temperature data, there is no possibility to perform the relevant detailed analysis of discrepancies. The deviation of the vibrational temperature

profile obtained on the basis of the data by *Kaye and Kumer* [1987] from kinetic temperature is not so large as for the FASCOD3P data, and does not exceed 5 K at the altitude of 30 km. The magnitude of the non-LTE effect in the mesosphere was not reported in the paper by *Kaye and Kumer* [1987].

In the calculations performed in the frame of the present work, we used the vibrational temperature profiles for NO borrowed from FASCOD3P dataset due to the following reasons:

- the total altitude range of interest is covered by these profiles;
- the values of T_v are larger than ones obtained from the data by *Kaye and Kumer* [1987], so there is the possibility to estimate the upper limit of the influence of non-LTE effect on the limb radiance measurements;
- we had no other data on vibrational temperatures at our disposal (except the vibrational temperature profile calculated from the data by *Kaye and Kumer* [1987]).

The vertical distribution of NO which we used in our calculations has been borrowed from the model AFGL-86 [*Anderson et al.*, 1986]. We did not take into account the diurnal variations of NO concentration, keeping in mind, however, that at night, there is, for all practical purposes, no NO in the stratosphere, since it is converted to NO_2 within minutes after sunset by reactions [*Kaye and Kumer*, 1987]:

$$NO + O_3 \rightarrow NO_2 + O_2$$
$$NO + ClO \rightarrow NO_2 + Cl$$

Below we shall refer to **Figures 2.1-2.3** when analyzing the optical properties of the limb paths and the peculiarities of the formation of outgoing limb radiation in the CO_2, O_3, and NO bands.

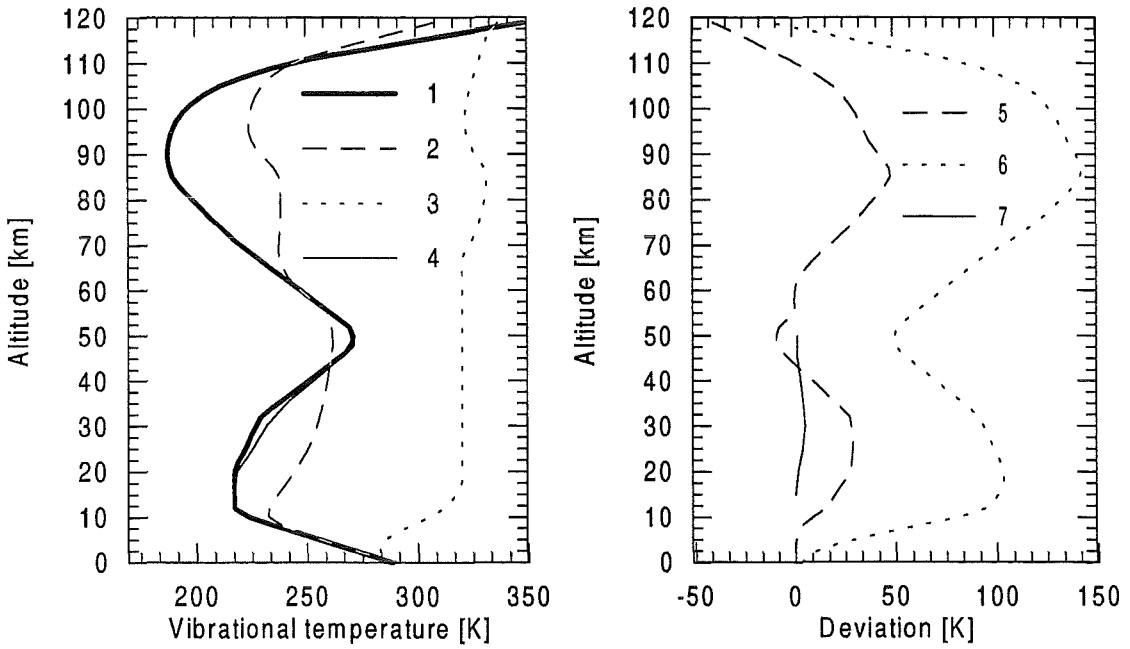

Fig. 2.3 Vibrational temperatures (T_v) for NO states X1/2-1 and X1/2-2 (left panel) and the deviations from the kinetic temperature (right panel).

1: kinetic temperature;
2: T_v (X1/2-1), FASCOD3P data;
3: T_v (X1/2-2), FASCOD3P data;
4: T_v (X1/2-1), calculated using data from *Kaye and Kumer* [1987];
5: $T_v - T_{kin}$ (X1/2-1), FASCOD3P data;
6: $T_v - T_{kin}$ (X1/2-2), FASCOD3P data;
7: $T_v - T_{kin}$ (X1/2-1), calculated using data from *Kaye and Kumer* [1987]

3. Computational tool.

The SPIRT-NLC computer code, the special line-by-line tool for the simulations of non-LTE limb atmospheric radiance, was applied to the investigation of the influence of non-LTE effects on the MIPAS measurements. The physical basis and the computing algorithm of the code are described in detail in the work by *Hollweg et al.* [1995].

The general scheme of calculations is as follows:

1. On the basis of the non-LTE atmospheric model and the line parameter data, the vertical profiles of non-LTE absorption coefficients and source functions are calculated. The line parameter data were taken from HITRAN database, 1992 edition [*Rothman et al.*, 1992].
2. On the basis of the precalculated vertical profiles of absorption coefficients and source functions, the monochromatic limb radiance spectra are calculated for the desired geometry.
3. The monochromatic spectra are degraded by the instrument spectral function in order to model the finite resolution spectra.

One of the principal advantages of SPIRT-NLC is the possibility to calculate the weighting functions (variational derivatives of limb radiance with respect to atmospheric parameters, including vibrational temperatures) which are suitable for solving the inverse problems of remote sensing by the optimal estimation method. The study of the problem of pressure-temperature retrievals from the limb radiance measurements in spectral microwindows was based on such approach. We applied the upgraded version (2.0) of SPIRT-NLC. This version contains the coded algorithm of the joint retrieval of the vertical profiles of kinetic temperature, gaseous composition and vibrational temperatures of the states of molecules from spectrally resolved limb emission measurements. Such multi-parameter approach was applied recently to the numerical estimation of the accuracy of the retrieval of a set of parameters (including non-LTE ones) from the measurements in 9-15 μm region, where the non-LTE features of carbon dioxide and ozone are displayed [*Timofeyev et al.*, 1995; *Kostsov et al.*, 1995]. In the paper by *Timofeyev et al.* [1992] one can find the detailed description of the multi-parameter approach and the discussion of its applicability.

4. The non-LTE effect in balloon-borne measurements.

This section contains the results of the study of the possibility to detect non-LTE effects in the atmosphere using limb-viewing geometry from balloon platforms. While selecting the MIPAS experimental balloon campaign being suitable for the analysis with account for non-LTE effect, we have used the following criteria:

- the maximal balloon height;
- the maximal tangent heights of observations;
- the presence of day-time measurements.

Campaigns in 1989, 1990, January 1992, March 1992 have been reviewed. It appeared that the campaign in 1990 was the most suitable for the considerations. Among the numerous data obtained in this campaign we have chosen the spectrum corresponding to the balloon height 39.54 km and tangent height 32.14 km, which was measured early in the morning. Unfortunately no spectra were available for day time. The resolution (apodized) was estimated to be 0.076 cm^{-1}. The accuracy of single spectrum measurement was estimated to be 0.8 $mW/(m^2 sr\ cm^{-1})$. In the case under consideration 18 spectra were averaged, so we have assumed the accuracy (NESR) to be 0.2 $mW/(m^2 sr\ cm^{-1})$.

Figure 4.1 presents the experimental spectra under consideration in the wavenumber region 910-990 cm^{-1}. In the region 910-960 cm^{-1} the spectrum structure is determined mainly by CO_2 lines of the transition 00011-10001, and the short-wave part of spectrum (960-990 cm^{-1}) is determined by the great number of lines belonging to ozone vibrational bands. It can be clearly seen that the data contain a lot of negative values between the lines due to the noise. We stress, that the noise appeared to increase with the shift towards the short-wave part of the interval because of the filter which has been used in the process of measurements (in this area the filter transmittance function dropped).

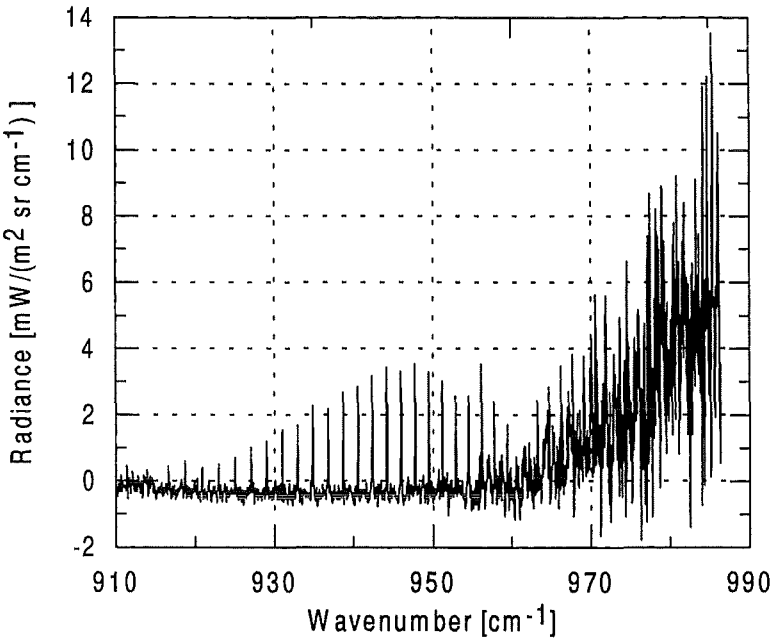

Fig. 4.1 Limb radiance experimental spectrum. Campaign 1990. Balloon height 39.54 km. Tangent height 32.14 km. Spectral region 910-990 cm^{-1}. Spectral resolution 0.076 cm^{-1}.

At the first step of investigations we simulated the limb radiance spectra in order to estimate the magnitude of the non-LTE effect and in order to locate the wavenumber interval of the most interest. For the "non-LTE effect" in radiance we assumed the difference between radiance values calculated for 2 models: the non-LTE model comprising carbon dioxide and ozone and the same model where vibrational temperatures were set equal to kinetic temperature. For the simulations we took the balloon height (39.54 km) and the elevation angles similar to ones, which appeared in the measurement scenario of the spectrum under consideration. The geometry characteristics are given in the **Table 4.1**. The last row of the table presents the characteristics for satellite limb viewing geometry just for the illustration of the differences in optical path length when the same tangent height is tracked.

Table 4.1 Geometry and limb path characteristics used for the simulations of limb radiance spectra.

Balloon height [km]	Elevation angle [deg]	Tangent height [km]	Total path length [km]
39.54	-3.100	30.16	1392.00
39.54	-2.920	31.21	1366.00
39.54	-2.752	32.14	1242.71
39.54	0.0	39.54	986.50
39.54	+3.000	-	706.50
39.54	+15.000	-	271.15
115.0	-9.168	32.14	2067.34

Figure 4.2 contains the calculated non-LTE effect (non-LTE radiance minus LTE one, as defined above) in the spectral interval 950-990 cm^{-1} for the balloon height 39.54 km and 4 elevation angles: -3.1^0, -2.92^0, 0^0, $+15^0$. Spectral resolution in all simulations described in this section was taken equal to 0.076 cm^{-1}. The results which are shown lead to the following conclusions:

a) The non-LTE effect increases with the shift to the larger wavenumbers, where the lines belonging to ozone hot bands are located.
b) The maximum non-LTE effect takes place when the elevation angle is close to -2.92^0.
c) The behavior of ozone spectra with the increasing of the elevation angle differs from the behavior of CO_2 spectra. For the negative elevation angles only 3 CO_2 lines in the interval 950-955 cm^{-1} are clearly distinguishable on the background of ozone spectra. But when the elevation angle is set to $+15^0$, the ozone spectrum "drops" down, and practically only P and R branch lines of CO_2 transition 00011-10001 remain intensive. This is explained by the fact that for up-looking geometry the contribution of lower atmospheric layers to the radiance is not so large as for limb viewing, and the contribution of upper layers becomes considerable. Ozone concentration decreases more quickly with altitude than the CO_2 concentration. That is why the emission of CO_2 is prevailing in this spectral interval for up-looking geometry.
d) The non-LTE effect exceeds the NESR=0.2 $mW/(m^2\ sr\ cm^{-1})$ for the elevation angle -2.92^0 only in the spectral interval ν>980 cm^{-1}. If we consider these effect as a "signal" then the signal-to-noise ratio appears to be rather small - not greater then 1.8 in the interval 980-990 cm^{-1}. Taking into account the fact of noise increase in this interval when MIPAS measurements were carried out, we can arrive to the conclusion that non-LTE effect can not be detected in the 1990 campaign data.

Though during the campaign in 1990 there were no spectra available in the region closer to the center of ozone band, it is interesting at least to simulate such an experiment. The example of this simulation is given in **Figure 4.3**, where the non-LTE effect is shown in the interval 990-

1030 cm^{-1} for the balloon height 39.54 km and tangent height 32.14 km. If NESR is assumed to be equal to 0.2 $mW/(m^2\ sr\ cm^{-1})$, then the signal-to-noise ratio in this case can reach the values up to 3 in the centers of the intensive lines of ozone hot bands. That means the possibility to detect the non-LTE effect, because in some cases the averaging of spectra while processing the experimental data can provide the NESR even less then 0.2 $mW/(m^2\ sr\ cm^{-1})$.

In order to investigate the fine structure of non-LTE effects when various elevation angles are used, we present **Figure 4.4**, where the narrow spectral interval 1005.5-1006.5 cm^{-1} is shown. The maximum in **Figure 4.4** corresponds to the strong line belonging to the ozone hot transition 003-002. The results, which are shown, confirm the above made conclusion on the

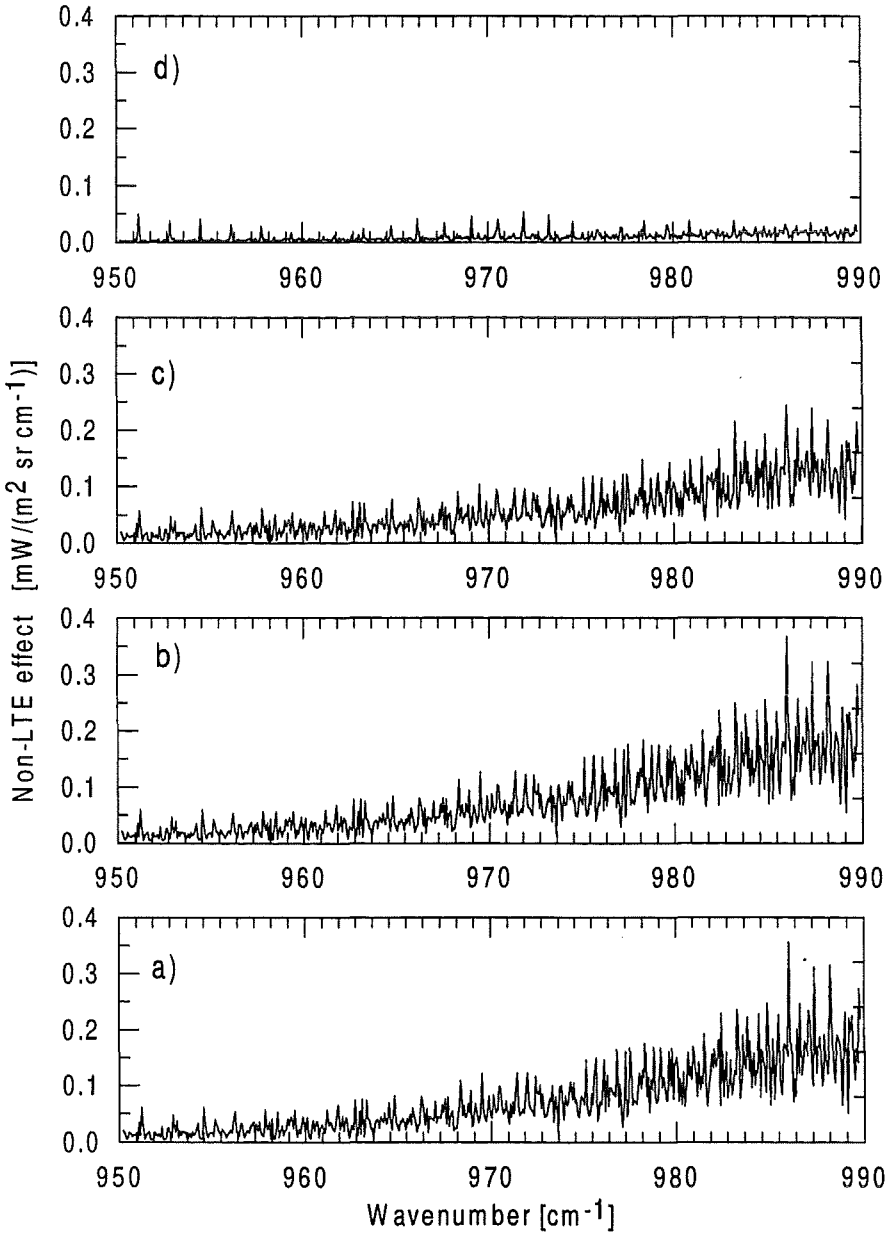

Fig. 4.2 The non-LTE effect estimated for the limb viewing geometry from a balloon platform. Balloon height 39.54 km. Spectral region 950-990 cm^{-1}. Elevation angles: -3.1° (a), -2.92° (b), 0° (c), +15° (d).

optimal value of the elevation angle to be about -2.9^0. With the change of the elevation angle there is practically no transformation of the form of the spectrum. Only for the wavenumber 1006.03 cm^{-1}, corresponding to the fundamental transition line, the change of angle from -3.1^0 to 0^0 gave an increase of the non-LTE effect which is negligibly small. For the comparison, the non-LTE effect which is estimated for the space-borne measurements, is also shown in **Figure 4.4**. This effect appeared to be about 35% higher than that for balloon-borne measurements.

For the comparison of the magnitude of non-LTE effect for balloon-borne and space-borne measurements we investigated also the second narrow interval containing the single CO_2 line of the transition 00011-10001 (the narrow intervals have been taken in order to reveal the fine structure of spectrum). **Figure 4.5** shows the radiance and the non-LTE effect for the interval 949.35-949.60 cm^{-1} where the CO_2 line is located. As it can be seen, in case of CO_2 spectrum and the tangent height 32.14 km, the non-LTE effect increases noticeably when the spectrum is observed from a satellite in comparison with the balloon geometry. The increase can be estimated by a factor of 4 while in case of the ozone spectrum the increase was ~35%. This is due to the intensive CO_2 emissions from the upper atmospheric layers. For the balloon geometry the NESR of 0.2 mW/(m^2 sr cm^{-1}) is not low enough to detect the non-LTE effect.

The results, which are presented lead to the following conclusions:

- With respect to the magnitude of radiance, the non-LTE effect is rather small for tangent height 32.14 km and constitutes in its maximum 3-4% of the radiance value. Nevertheless, if NESR is equal to 0.2 mW/(m^2 sr cm^{-1}), the effect could be detectable on the background of noise both from balloon-borne and space-borne platforms.
- The maximal non- LTE effect is observed in the lines of ozone hot transitions.
- The balloon and satellite spectra for the tangent height 32.14 km are very close to each other despite the fact that optical path length for a satellite viewing is nearly 2 times greater than

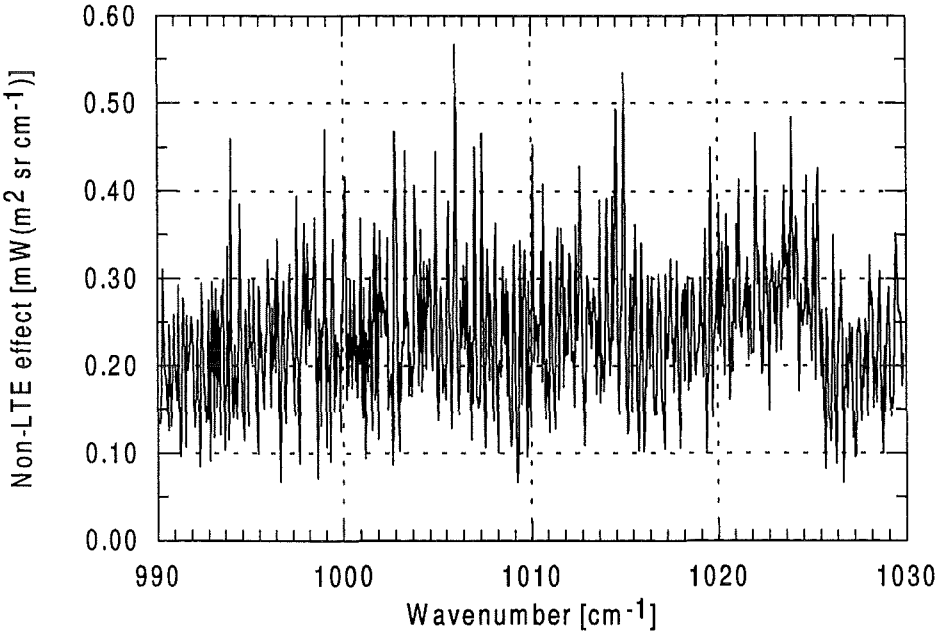

Fig. 4.3 The non-LTE effect estimated for the limb viewing geometry and balloon platforms. Balloon height 39.54 km. Tangent height 32.14 km. Spectral region 990-1030 cm^{-1}.

that for balloon viewing. The same is true also for the non-LTE effect. It is only ~35% higher for satellite observation geometry.

The main conclusion, therefore, is the following: the NESR of 0.2 mW/(m^2 sr cm^{-1}) is sufficient in order that the non-LTE effect in the ozone 9.6 μm band emissions can be detected by balloon limb measurements. In order to detect the non-LTE effect in the CO_2 10 μm band emissions from the balloon platforms it is necessary to increase the sensitivity of the instrument at least to the value of NESR 0.05 mW/(m^2 sr cm^{-1}). This conclusion is valid for the spectral resolution of measurements of 0.076 cm^{-1} and measurement scenario which were characteristic for the MIPAS-B balloon campaign.

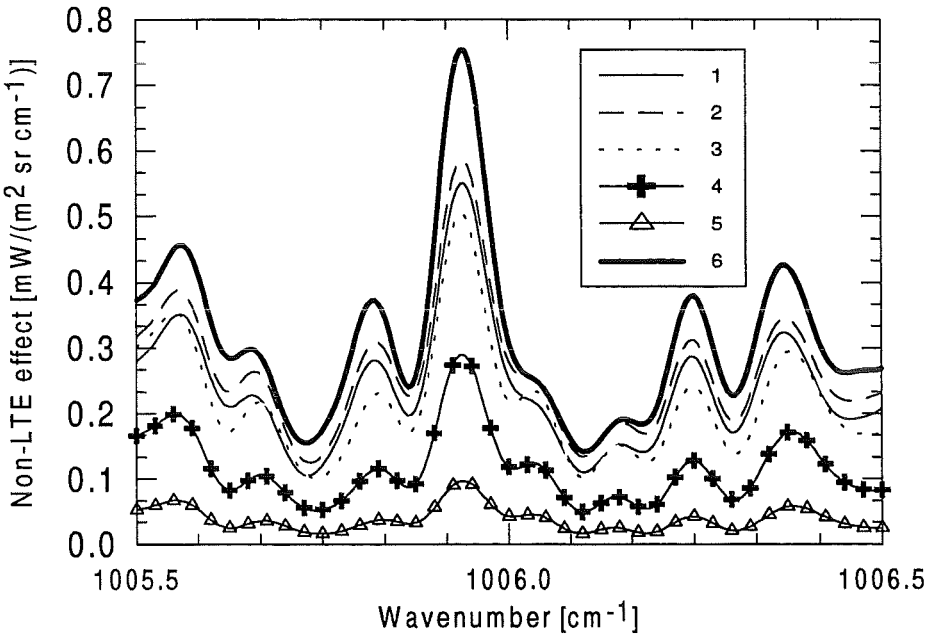

Fig. 4.4 The estimated non-LTE effect depending on the elevation angle for the balloon height 39.54 km. A narrow spectral region containing ozone lines. The non-LTE effect for space-borne measurements is presented for comparison.

Line No	1	2	3	4	5	6
Elevation angle [deg]	-3.1	-2.752	0.0	+3.0	+15.0	space-borne measurements
Tangent height [km]	30.16	32.14	39.54	-	-	32.14

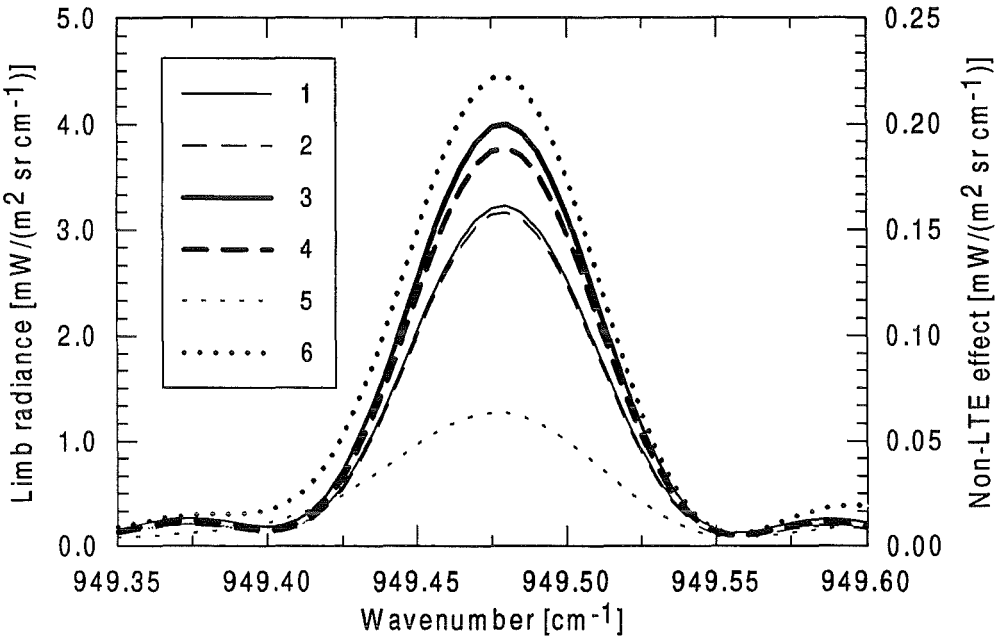

Fig. 4.5 Simulated limb spectra and non-LTE effect for the space-borne and balloon-borne measurements for tangent height 32.14 km. Balloon height was taken equal to 39.54 km. A narrow spectral interval contains a carbon dioxide line. Radiance (left scale): 1-non-LTE (balloon), 2-LTE (balloon), 3-non-LTE (satellite), 4-LTE (satellite). Non-LTE effect (right scale): 5-balloon, 6-satellite.

5. The non-LTE effect in case of space-borne measurements.

5.1 CO_2 and O_3 bands.

The investigation of the influence of non-LTE effect on the MIPAS space-borne measurements was performed for the spectral region 680-980 cm^{-1}, where the microwindows are located, which were preselected for the purpose of the pressure-temperature (p-T) retrievals [*Clarmann et al.*, 1994].

The list of lines preliminary compiled for the use in p-T retrievals by *Clarmann et al.* [1994] has been analyzed, and the following characteristics have been added: isotope identifier, line intensity, corresponding vibrational transition and branch. The values of the enumerated parameters have been taken from HITRAN database, 1992 edition. The non-LTE effect depends upon the line intensity and upon the populations of the corresponding upper and lower vibrational levels. Therefore the most intensive lines have been chosen for analysis which represent isotopes 1(626), 3(628), 4(627) of carbon dioxide under non-LTE and all major vibrational transitions (see **Table 5.1**). Transitions are given in the AFGL notation which was accepted in the present study. The microwindows are marked with respect to the atmospheric altitude (47 km, 29 km, 11 km) which is supposed to be sounded using spectra measured in these microwindows.

The limb radiance profiles were simulated for the centers of the above listed lines in the tangent height range 30-110 km. Both LTE and non-LTE cases have been considered. The limb radiance profiles have been plotted together with the non-LTE effect, which is defined (like in the previous sections) as LTE values minus non-LTE values or vice versa if it is stated explicitly. Since the logarithmic scale was used, the positive values of the non-LTE effect are marked with "+" sign and the negative values are marked with "-" sign.

Table 5.1 CO_2 spectral lines chosen for analysis.

Wavenumber [cm^{-1}]	Iso-tope	Line intensity [cm^{-1}/mol cm^{-2}]	Lower state energy [cm^{-1}]	Transition	Branch
Microwindow: 686.22-686.34 (47 km), 686.22-686.35 (29 km)					
686.2576	**4**	**4.34E-23**	**286.1604**	**01101-00001**	**R27**
Microwindow: 690.33-690.41 (47 km)					
690.3637	**1**	**1.07E-19**	**316.7698**	**01101-00001**	**R28**
Microwindow: 690.83-690.98 (29 km)					
690.9436	**3**	**1.02E-22**	**517.4328**	**01101-00001**	**R33**
Microwindow: 695.47-695.67 (47 km), 695.48-695.66 (29 km)					
695.5132	**1**	**2.82E-21**	**1105.5066**	**02201-01101**	**R33**
Microwindow: 701.39-701.50 (47 km)					
701.4119	**1**	**7.83E-23**	**1977.0937**	**03301-02201**	**R40**
Microwindow: 957.75-957.86 (29 km)					
973.2885	**1**	**2.29E-23**	**1494.3072**	**00011-10001**	**R16**

For the sake of the comparison, the limb radiance profile has been simulated also for the center of the strong Q16 line (ν=667.6614 cm^{-1}), where the non-LTE effect can be very strong, though this line does not belong to any preselected microwindow. The results of the calculations for this "reference" line are given in **Figure 5.1** (part "a"). Part "b" of the **Figure 5.1** shows limb radiance profiles for the most intensive CO_2 line which is included in the microwindows. The most attention is to be paid to the non-LTE effect profiles, which reflect mainly the behavior of the vibrational temperatures of different levels with respect to the kinetic temperature. For the fundamental transition lines of the main isotope (**Figure 5.1**), the non-LTE effect is always positive, since T_v is less than T_{kin} over the entire altitude region under consideration. The non-LTE effect for the Q16(01101-00001) line exceeds the NESR of MIPAS (see **Table 1.1**) by the factor of 2 for all tangent heights from 30 up to 110 km. For the line R28(01101-00001) the non-LTE effect is not emphasized so strongly, but still it is greater than NESR in the tangent height regions 30-50 km and 100-110 km. Similar behavior of the non-LTE effect is characteristic also for the 02201-01101 transition lines, since T_v of the level 02201 does not exceed the kinetic temperature. But the non-LTE contribution is smaller. If we consider the fundamental transition for the minor isotopes, the non-LTE effect profile changes its sign, because the corresponding vibrational temperatures of the level 01101 exceed T_{kin} in the layers 70-105 km and have the lower values above 105 km. Therefore the non-LTE limb radiance in the tangent height region 65-95 km exceeds the LTE one. But for the lines of the minor isotopes the non-LTE effect is much smaller than NESR for all tangent altitudes. The same holds true for the 03301-02201 lines of the major isotope, where non-LTE effect becomes negative for the tangent heights 70-90 km where T_v of the state 03301 exceeds T_{kin}.

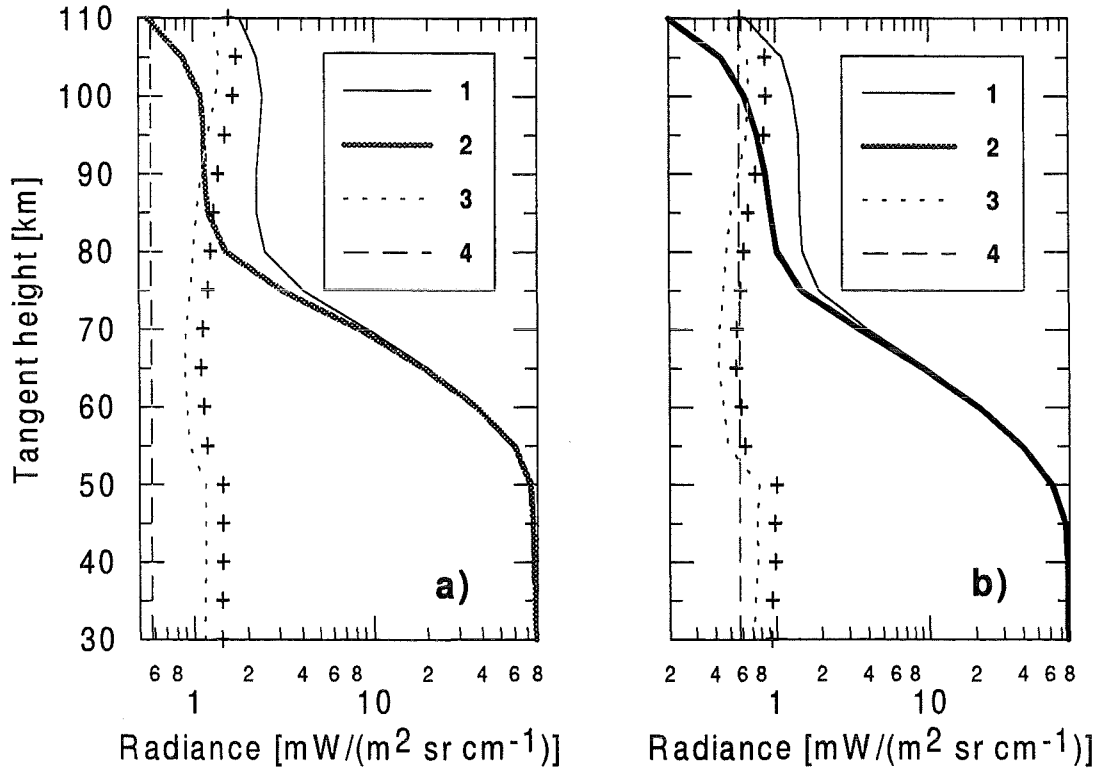

Fig. 5.1 Simulated limb radiance profile (LTE and non-LTE) for the center of CO_2(626) Q16 line at ν=667.6614 cm^{-1} (part a) and R28 line at ν=690.3637 cm^{-1} (part b). Transition 01101-00001. Spectral resolution 0.05 cm^{-1}.

1 - LTE radiance;
2 - non-LTE radiance;
3 - non-LTE effect;
4 - NESR of the MIPAS measurements.

The situation changes considerably in the spectral domain of the 00011-10001 transition (**Figure 5.2** "a"). The population of the level 00011 is strongly enhanced for the non-LTE case and the corresponding T_v is greater than T_{kin} by about 100 K in the vicinity of 80-90 km. As a consequence, the non-LTE limb radiance is much greater than the LTE one starting from the tangent altitude of about 60 km. The NESR in this spectral region is 0.15 mW/(m^2 sr cm^{-1}) which is about 4 times less than in 15 μm region. Therefore, the non-LTE effect exceeds NESR up to 90 km by a factor of 3-4.

Test calculations have been performed in order to estimate possible influence of the emissions not only of CO_2 lines, but also of ozone non-LTE lines on the p-T retrieval. The microwindows have been selected in such a way that they don't contain the strong lines of the interfering gases. The test calculations were performed for the remaining 2 strongest lines belonging to ozone transitions 010-000 and 110-100. The limb radiance profiles for the 110-100 transition line is shown in **Figure 5.2** "b". As the non-LTE effect is much less than NESR for these lines it will be negligibly small for sure for the less intensive lines still contained in the selected microwindows.

The obtained results lead to the following conclusions. In the microwindows located in the 15 μm CO_2 band the non-LTE effect appears to have no significant influence on the limb radiance and hence on p-T retrievals. In the 10 μm CO_2 band this effect is much stronger and in connection with the lower NESR in this spectral region it can influence to a certain degree the results of p-T retrievals if not accounted for. Hence, from the point of eliminating possible non-LTE effect, the microwindows in the 15 μm region were set optimally by *Clarmann et al.* [1994]. However, the utilization of the microwindows containing CO_2 "laser" lines has to be checked more carefully, and, if necessary, a corresponding corrective algorithm should be developed.

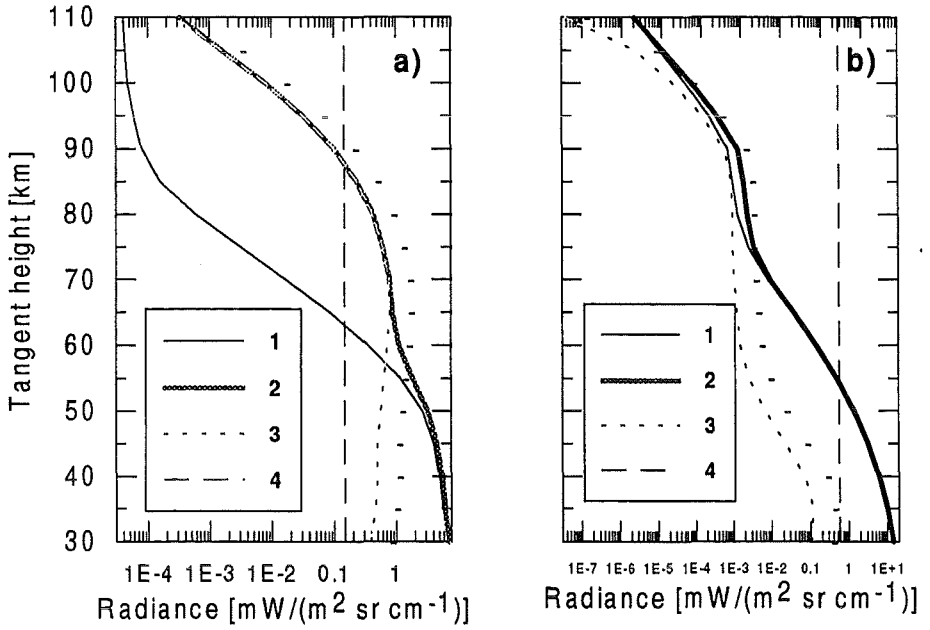

Fig. 5.2 Simulated limb radiance profiles (LTE and non-LTE) for the center of CO_2(626) R16 line at ν=973.2885 cm^{-1}, transition 00011-10001, (part a) and ozone line at ν=709.6241 cm^{-1}, transition 110-100 (part b). Spectral resolution 0.05 cm^{-1}.
1 - LTE radiance;
2 - non-LTE radiance;
3 - non-LTE effect;
4 - NESR of the MIPAS measurements.

5.2 NO bands.

At the first stage of investigations, we analyzed the formation of outgoing non-LTE limb radiance for the monochromatic case. We have chosen for the analysis 2 strong spectral lines belonging to the vibrational transitions X1/2-1 → X1/2-0 and X1/2-2 → X1/2-1.

For the fundamental transition X1/2-1 → X1/2-0 we have chosen the R6 line centered at ν_0=1900.0709 cm^{-1}. The line intensity is $6.0 \cdot 10^{-20}$ cm^{-1}/molecule cm^{-2}. Simulated profiles of non-LTE and LTE limb radiances and other optical characteristics calculated at the center of this line are shown in **Figure 5.3**. The tangent altitude z_t varied from 1 to 119 km. The obtained results lead to the following conclusions:

- The non-LTE effect (the difference between LTE and non-LTE limb radiance values) changes its sign several times. For z_t less than 42 km the non-LTE limb radiance exceeds considerably the LTE one and the non-LTE effect can reach 0.63 mW/(m^2 sr cm^{-1}). The non-LTE radiance is greater than LTE radiance also for the tangent altitude region 54-104 km. For the tangent altitude range 42-53 km and 104-119 km the non-LTE radiance is less than LTE radiance. This behavior of the non-LTE effect follows practically exactly the behavior of the deviation of the vibrational temperature T_v(X1/2-1) from the kinetic temperature (see **Figure 2.3**) due to the transparency of the optical paths.
- The atmosphere is semi-transparent for all limb paths considered (tangent altitudes from 1 to 119 km). The optical depth does not exceed 1.5, and the transmittance is never less than 0.25.

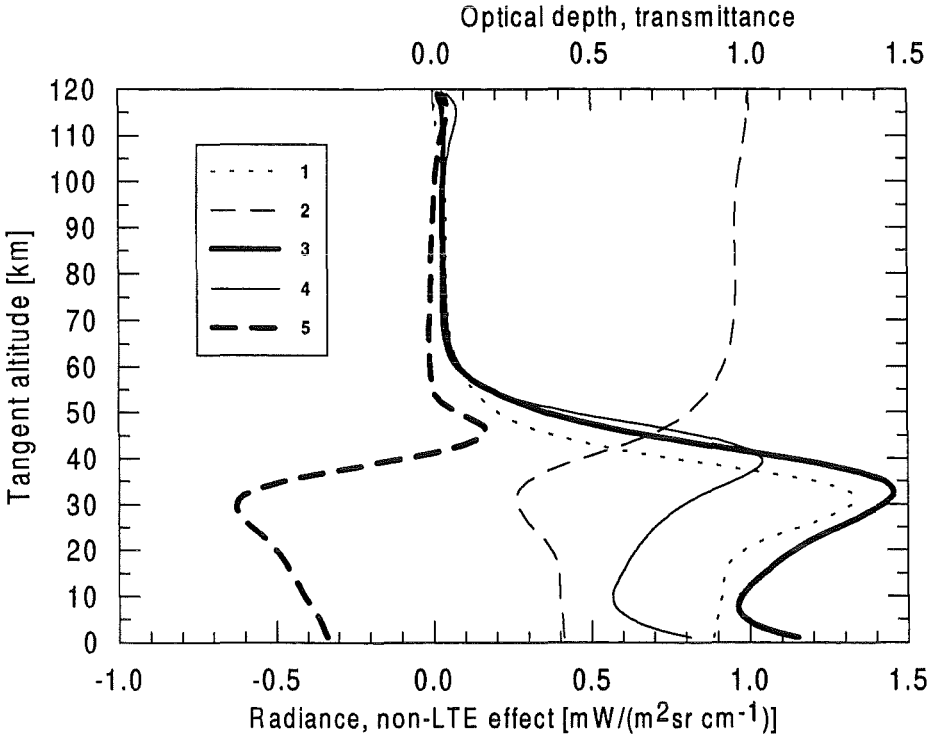

Fig. 5.3 Simulated profiles of non-LTE and LTE limb radiances and other optical characteristics calculated at the center of R6 line (ν_0=1900.0709 cm^{-1}) of NO fundamental transition X1/2-1→X1/2-0.

1 - optical depth;
2- transmittance
3 - non-LTE radiance [mW/(m^2 sr cm^{-1})];
4 - LTE radiance [mW/(m^2 sr cm^{-1})]
5 - non-LTE effect [mW/(m^2 sr cm^{-1})]

The atmosphere is the most opaque at the path corresponding to the tangent altitude 30 km since there is a local maximum of NO number density in the vicinity of 35 km.

- The limb radiance profiles both for LTE and non-LTE conditions exhibit similar behavior with 3 local maximums at tangent altitudes 1 km, 30 km and 115 km. The largest maximum is for the tangent altitude 30 km and is due to the local maximum of NO number density.
- Since the atmosphere is transparent in the considered spectral line, there are no line saturation features in the line shapes calculated for different tangent altitudes.

For the first hot band X1/2-2→X1/2-1 we have chosen the R6 line centered at ν_0=1871.7257 cm^{-1}. The line intensity is $1.44 \cdot 10^{-23}$ cm^{-1}/molecule cm^{-2}. Simulated profiles of non-LTE and LTE limb radiances at the center of this line are shown in **Figure 5.4**. The tangent altitude z_t varied from 1 to 119 km.

In comparison with the line of the fundamental transition, the non-LTE enhancement of limb radiance for the first hot transition is more pronounced. The maximal non-LTE effect appears to be at the tangent altitude 30 km, where the radiance has its maximum. The optical depth and transmittance are not shown in the Figure since the optical depth values are very small, and the transmittance is close to unity. The behavior of the non-LTE effect is in accordance with the vibrational temperature profiles (see **Figure 2.3**): the deviation of T_v(X1/2-2) from the kinetic temperature can reach 100 K.

In the analysis of limb radiance simulations for the case of finite spectral resolution, we take into account the characteristics of the MIPAS instrument (**Table 1.1**). The 4th and the 5th channels are located in the area of NO vibrational bands which are influenced by non-LTE. The noise equivalent spectral radiance (NESR) of MIPAS measurements in the 4th and 5th channels is estimated to be about 0.02 mW/(m^2 sr cm^{-1}). The apodized spectral resolution of measurements is expected to be 0.05 cm^{-1}. We performed our calculations with this value of the spectral resolution and the $Sinc^2$ spectral scanning function.

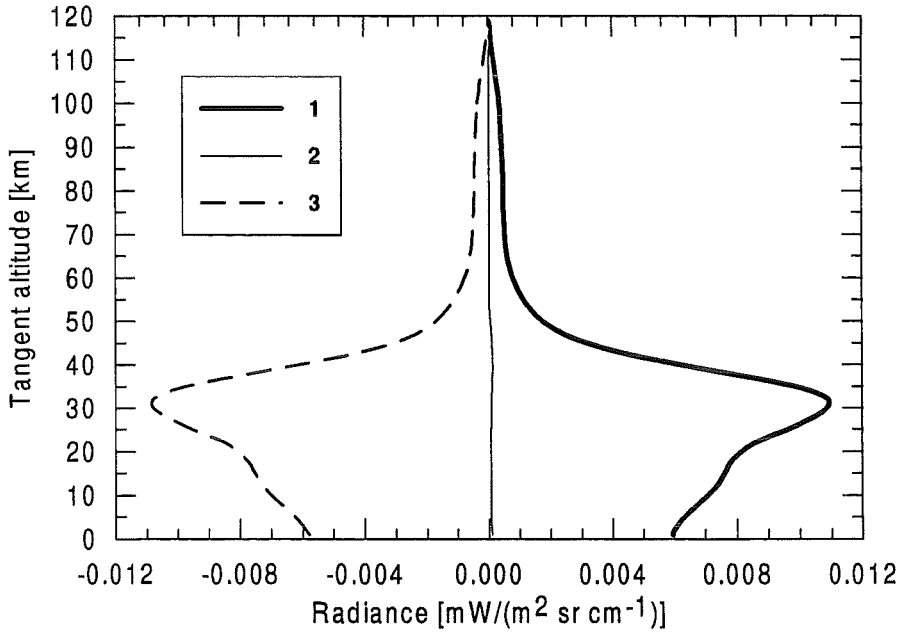

Fig. 5.4 Simulated profiles of non-LTE and LTE limb radiances and other optical characteristics calculated at the center of R6 line (ν_0=1871.7257 cm^{-1}) of NO first hot transition X1/2-2→X1/2-1.

1 - non-LTE radiance [mW/(m^2 sr cm^{-1})];
2 - LTE radiance [mW/(m^2 sr cm^{-1})]
3 - non-LTE effect [mW/(m^2 sr cm^{-1})]

First, we present the calculations of limb radiance spectra for the fundamental and first hot bands taken separately. Now we pass to the fundamental band. **Figure 5.5** shows the limb radiance profile calculated at wavenumber 1900.0709 cm^{-1}, which is the center of the fundamental transition line already analyzed in the monochromatic case.

The most important results concern the comparison between LTE and non-LTE radiances and between calculated non-LTE effect and the NESR of MIPAS measurements. The non-LTE radiance exceeds considerably the LTE radiance for the tangent altitudes up to 35 km. The non-LTE effect is about 0.15 $mW/(m^2\ sr\ cm^{-1})$ in the tangent altitude region 10-30 km and is greater than NESR by a factor of 7. In the area, where the non-LTE effect is positive ($z_t \approx 45$ km), it is also comparable with NESR. These results lead to a conclusion about the importance of accounting for non-LTE effects for the MIPAS measurements throughout the troposphere and stratosphere for the fundamental transition lines.

The limb radiance profiles were also calculated at the center of the strong line of the first hot transition (ν_0=1871.7257 cm^{-1}). The results are displayed in **Figure 5.6**. The transmittance is not shown in the figure since it is close to unity. Due to the large values of the vibrational temperature T_v(X1/2-2), the great enhancement of non-LTE radiance with respect to the LTE one is observed. However, both radiance values and non-LTE effect values are far below the NESR level of the MIPAS measurements (by a factor of 10). Therefore, the lines of the first hot transition appear to be even not detectable in measurements.

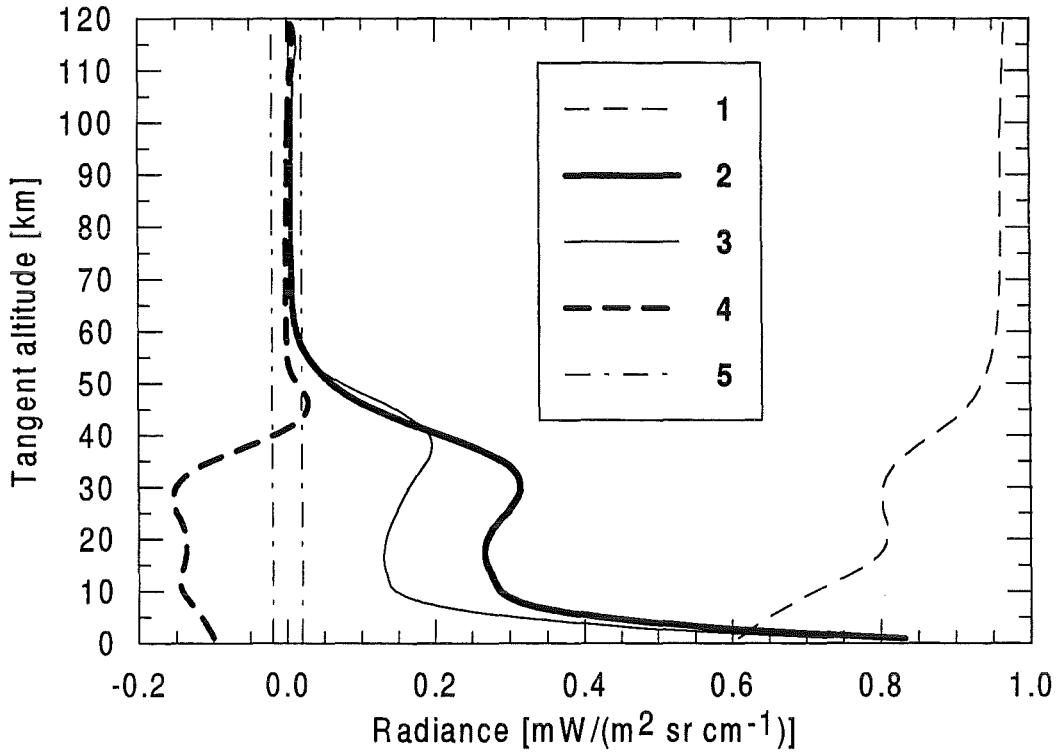

Fig. 5.5 Simulated profiles of non-LTE and LTE limb radiances and transmittance calculated at the center of R6 line (ν_0=1900.0709 cm^{-1}) of NO fundamental transition X1/2-1→X1/2-0.

1- transmittance
2 - non-LTE radiance [$mW/(m^2\ sr\ cm^{-1})$];
3 - LTE radiance [$mW/(m^2\ sr\ cm^{-1})$];
4 - non-LTE effect [$mW/(m^2\ sr\ cm^{-1})$];
5 - lines indicating the measurement corridor (NESR of MIPAS).

It is necessary to keep in mind, that NO has a lot of vibrational transitions which fall in the MIPAS measurement channels. In the **Table 5.2** we enumerate the most important of them from the point of line intensities. The transitions which were considered above are emphasized by bold typing.

The transition X3/2-1→X3/2-0 is the second most intensive. The deviation from LTE for this transition is accounted for in FASCOD3P computer code. However, we do not have the information, how the vibrational temperature for the state X3/2-1 is generated, since the corresponding FASCOD3P data contain the vibrational temperature profiles for the states with

Table 5.2 NO bands.

Transition	Wavenumber interval [cm^{-1}]	Sum of line intensities [cm^{-1}/molecule cm^{-2}]
X1/2-2→X3/2-1	1540 - 1777	1.175E-25
X1/2-1→X3/2-0	1566 - 1805	5.530E-22
X3/2-2→X3/2-1	1706 - 1944	3.767E-22
X1/2-2→X1/2-1	**1709 - 1943**	**7.034E-22**
X3/2-2→X1/2-1	1875 - 2112	2.562E-25
X3/2-1→X1/2-0	1903 - 2142	1.205E-21
X3/2-1→X3/2-0	1733 - 1974	1.585E-18
X1/2-1→X1/2-0	**1736 - 1972**	**2.945E-18**

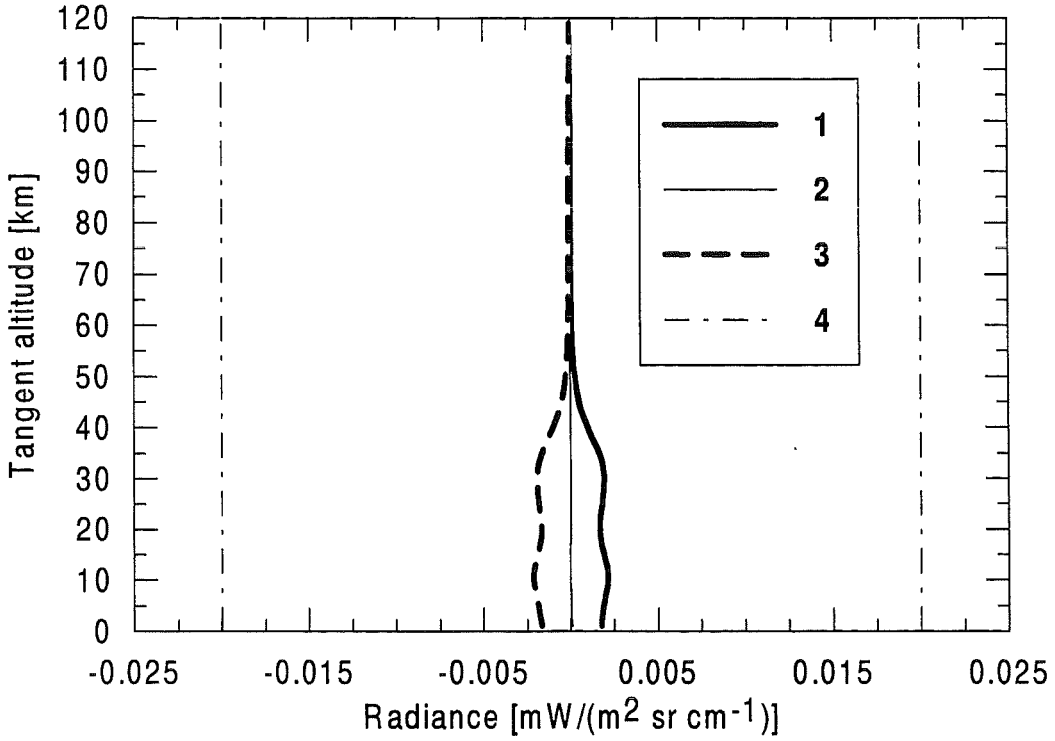

Fig. 5.6 Simulated profiles of non-LTE and LTE limb radiances and transmittance calculated at the center of R6 line (ν_0=1871.7257 cm^{-1}) of NO first hot transition X1/2-2→X1/2-1.
1 - non-LTE radiance;
2 - LTE radiance;
3 - non-LTE effect;
4 - lines indicating the measurement corridor (NESR of MIPAS).

energies 1876 cm^{-1} and 3724 cm^{-1} (these are the states X1/2-1 and X1/2-2).

In order to make an approximate estimation of the magnitude of possible non-LTE influence on the results of limb radiance measurements, we assumed the states X1/2-1 and X3/2-1 in the thermodynamic equilibrium between each other due to the close values of state energies. In this case the vibrational temperature profiles are essentially the same for both states. Then we performed calculations of the limb radiance profile for the R6 line of the transition X3/2-1→X3/2-0 (ν_0=1900.5157 cm^{-1}).

The results of limb radiance calculations are displayed in **Figure 5.7**. The behavior of limb radiance profiles, transmittance and non-LTE effect is naturally the same as for the line of the X1/2-1→X1/2-0 transition. Only the magnitude of radiances is less by a factor of 2, and the atmosphere is more transparent. Still, the non-LTE effect exceeds NESR of MIPAS up to z_t=40 km and is comparable with NESR in the vicinity of z_t=45 km.

There are many H_2O, CO_2 and O_3 bands overlapping with the NO bands in the MIPAS measurement channels. We shall consider the channel No 5 around the wavenumber 1900 cm^{-1}. In the tables III, IV, V, the most intensive vibrational bands of H_2O, CO_2 and O_3 are presented, which are influenced by non-LTE.

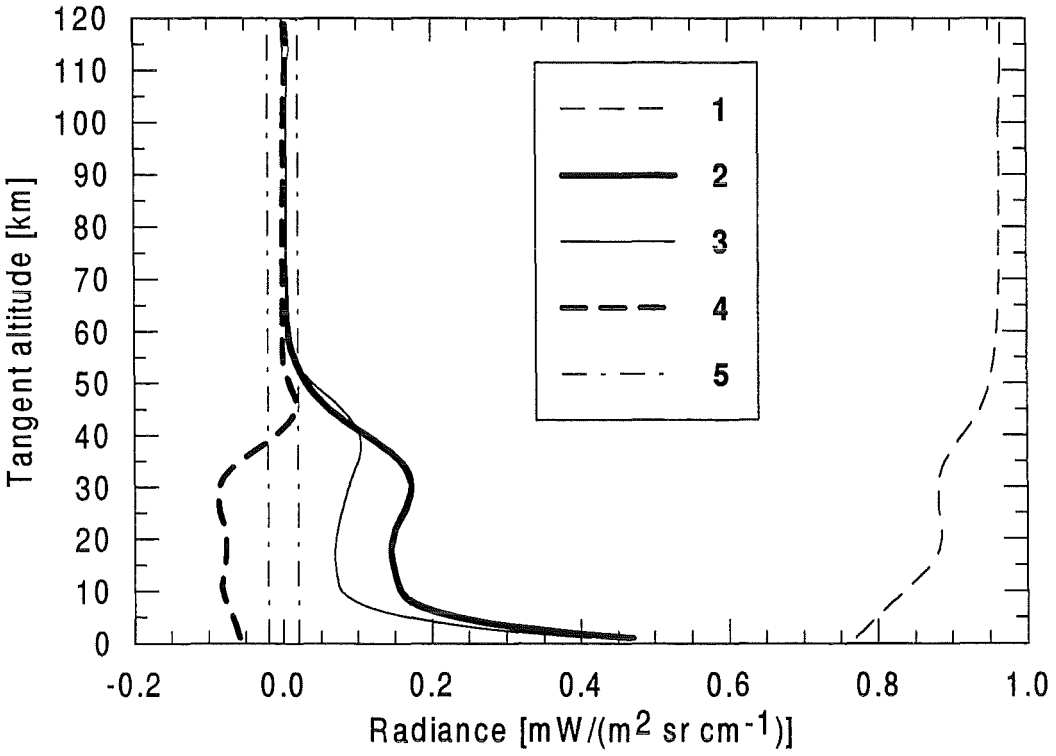

Fig. 5.7 Simulated profiles of non-LTE and LTE limb radiances and transmittance calculated at the center of R6 line (ν_0=1900.5175 cm^{-1}) of NO transition X3/2-1→X3/2-0. Spectral resolution 0.05 cm^{-1}.

1- transmittance
2 - non-LTE radiance [mW/(m^2 sr cm^{-1})];
3 - LTE radiance [mW/(m^2 sr cm^{-1})];
4 - non-LTE effect [mW/(m^2 sr cm^{-1})];
5 - lines indicating the measurement corridor (NESR of MIPAS).

Table 5.3 The most intensive H_2O bands overlapping with the NO bands.

Band center [cm^{-1}]	Transition	Wavenumber interval [cm^{-1}]	Number of lines	Sum of line intensities [cm^{-1}/molecule cm^{-2}]
1515.1630	030 → 020	1271 - 1932	121	5.135E-24
1556.883	020 → 010	945 - 2407	728	9.709E-21
1594.7498	010 → 000	782 - 2910	1763	1.058E-17
2062.306	100 → 010	1221 - 2520	402	1.820E-22
2161.183	001 → 010	1298 - 2612	365	2.626E-22

Table 5.4 The most intensive CO_2 bands overlapping with the NO bands.

Band center [cm^{-1}]	Transition	Wavenumber interval [cm^{-1}]	Number of lines	Sum of line intensities [cm^{-1}/molecule cm^{-2}]
1880.987	20003 → 01101	1828 - 1936	88	1.271E-23
1917.642	12202 → 01101	1867 - 1975	186	3.856E-23
1932.470	11102 → 00001	1871 - 1999	118	6.583E-22
2003.763	20002 → 01101	1952 - 2039	66	3.046E-24

Table 5.5 The most intensive O_3 bands overlapping with the NO bands.

Band center [cm^{-1}]	Transition	Wavenumber interval [cm^{-1}]	Number of lines	Sum of line intensities [cm^{-1}/molecule cm^{-2}]
1726.5225	011 → 000	1634 - 1927	3415	5.357E-20
1796.2619	110 → 000	1666 - 1963	3695	2.374E-20
1942.9509	003 → 100	1856 - 2094	1285	1.379E-21
2004.0042	003 → 001	1891 - 2086	1685	1.189E-21
2057.8908	002 → 000	1882 - 2278	5339	1.120E-19
2084.3082	111 → 010	1930 - 2221	2514	4.083E-20
2110.7843	101 → 000	1913 - 2322	5865	1.236E-18

It should be mentioned, that we included the most intensive bands between the levels for which the vibrational temperature profiles are available in FASCOD3P. As it can be seen, the spectral region of interest near 1900 cm^{-1} does not comprise the centers of the most of H_2O, CO_2 and O_3 bands. Only two CO_2 bands (20003-01101 and 12202-01101) are centered nearby, however these bands are relatively weak.

Figure 5.8 shows the total transmittance spectrum in the interval 1890-1910 cm^{-1} for the tangent height 10 km and the separate contributions to the total transmittance made by NO, O_3, CO_2, and H2O,. The largest contributions are due to the absorption by water vapor and carbon dioxide. Ozone has practically no influence on the transmittance. Nitric oxide contributes to the transmittance also not very significantly.

Figure 5.9 presents the limb radiance spectra for the tangent height 10 km, and also the contributions from atmospheric constituents which were calculated under the approximation of mono-gas atmosphere. Similar to the case of the transmittance, the total radiance is shown and the contributions made by single emitting gases are displayed. We stress that the calculations were performed for the complete non-LTE case, i.e. the deviations from local thermodynamic equilibrium were taken into account for all gases considered. It follows from the figure, that total limb radiance is determined by water vapor, carbon dioxide and nitric oxide. Ozone lines are beyond the level of measurement errors (NESR). The NO lines are quite strong and are clearly distinguishable on the background of H_2O and CO_2 lines.

The influence of the non-LTE effect is illustrated in **Figure 5.10** for the tangent height 10 km. The non-LTE effect was calculated as LTE radiance minus non-LTE one and the separate contributions from atmospheric species were calculated in the same way. The non-LTE effect from NO is dominant and reaches -0.15 mW/(m^2 sr cm^{-1}) in the line centers. The non-LTE effects from water vapor, carbon dioxide and ozone are far beyond the level of detectability (which we assume equal to NESR = 0.02 mW/(m^2 sr cm^{-1}). So, though nitric oxide is not the main contributor to radiance, its non-LTE effect is important in the considered spectral interval.

Figure 5.11 is similar to **Figure 5.10**, but the non-LTE effect was calculated for the tangent height 30 km. The non-LTE effect from NO remains dominant for this tangent height also, reaching the level of -0.15 mW/(m^2 sr cm^{-1}). The non-LTE effect from water vapor became much smaller than for the tangent height 10 km, the non-LTE effect for CO_2 became a little bit larger, however still remaining non-detectable. For ozone, the considerable growth of the non-LTE effect can be observed (approximately by a factor of 2), still it is lower than NESR of the MIPAS measurements.

Finally, we present **Figure 5.12**, where the non-LTE effect is presented for the tangent height 50 km. For this tangent height, it is beyond the level of detectability for all considered atmospheric species. However, contrary to the lower tangent altitudes, for z_t=50 km the non-LTE effects from ozone, NO and CO_2 become of the same order of magnitude.

Summing up the results of the limb radiance simulations for NO bands, we stress the main conclusion: the non-LTE effect can be detected in the MIPAS measurements in the tangent altitude range 1-40 km.

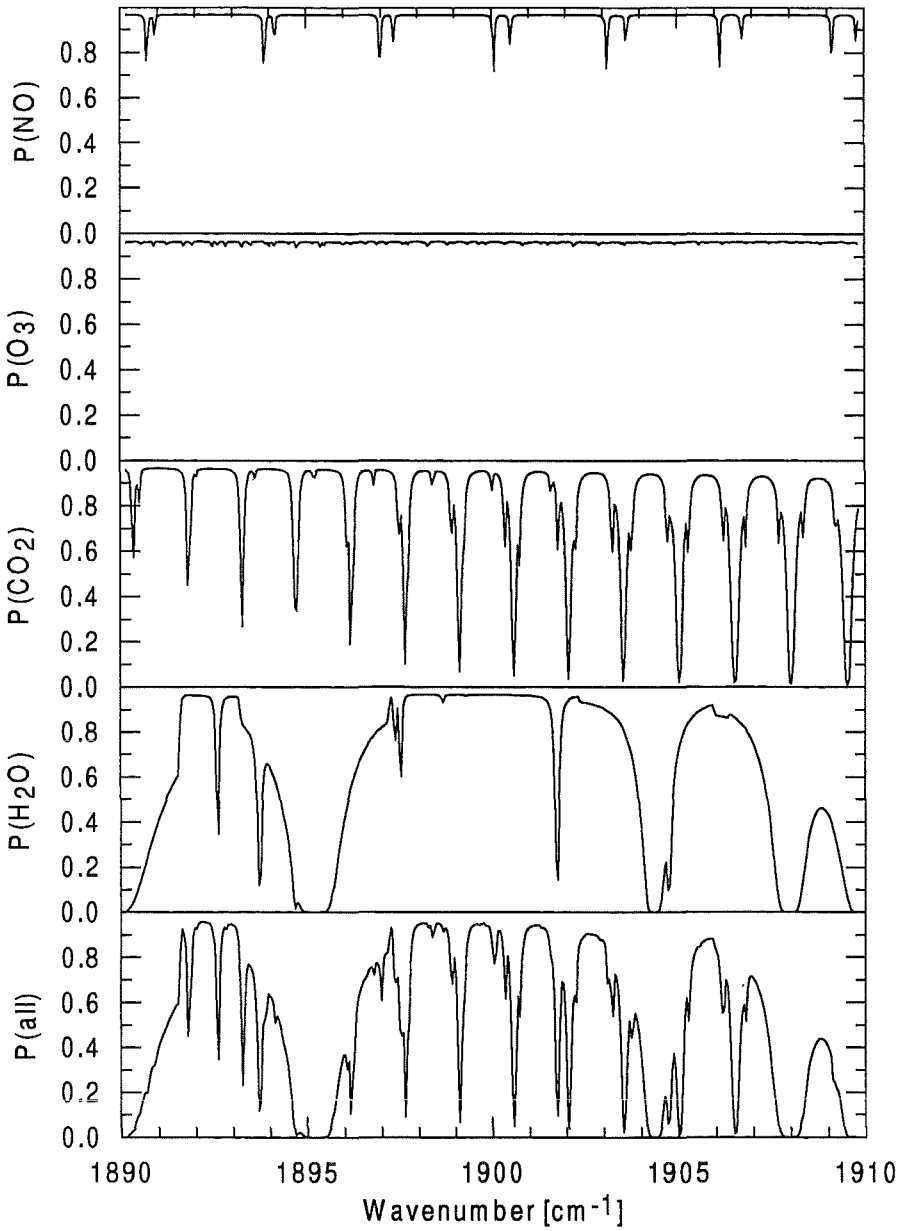

Fig. 5.8 The total transmittance P(all) on a limb path for the tangent height 10 km (lower panel) and the separate contributions from atmospheric species P(gas) (upper panels).

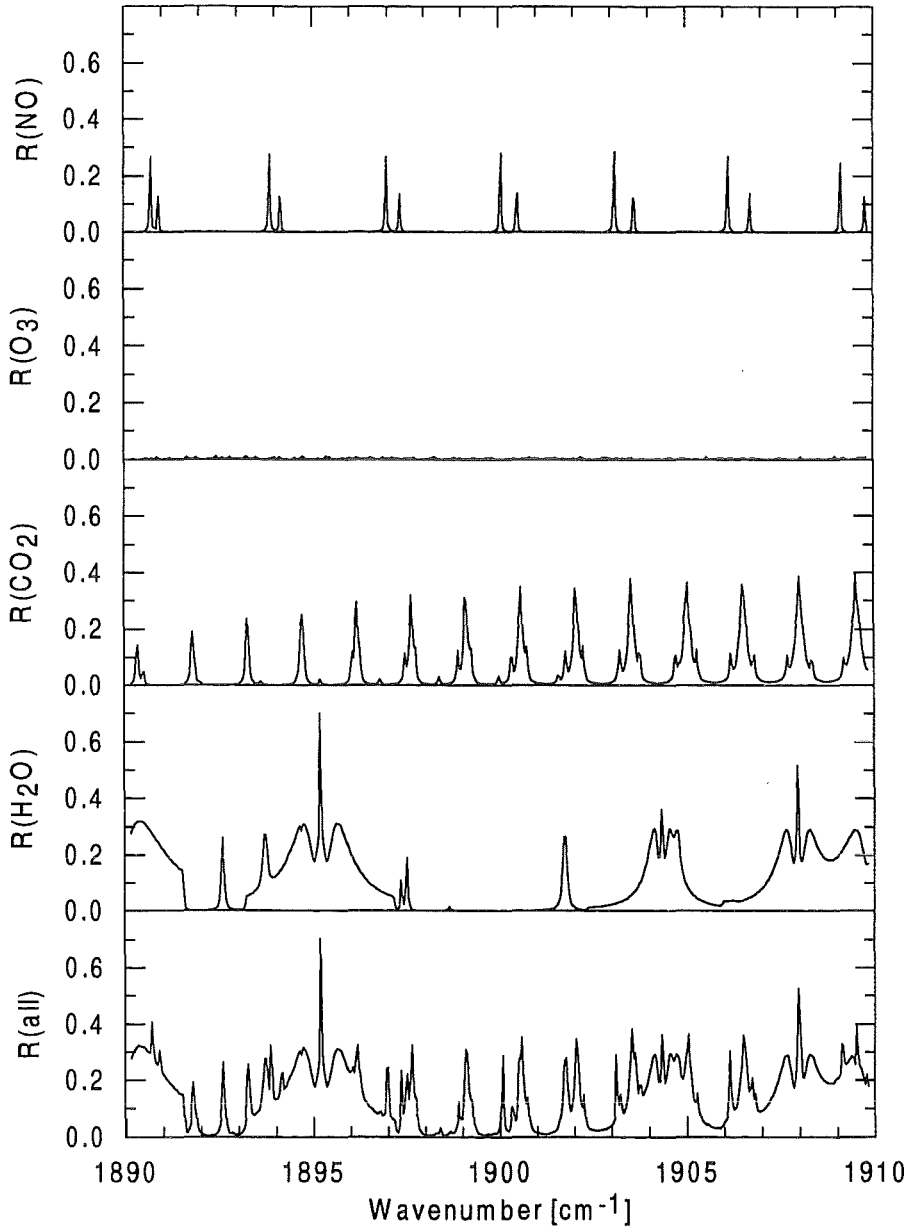

Fig. 5.9 The non-LTE emission spectrum R(all) [mW/(m^2 sr cm^{-1})] for the tangent height 10 km (lower panel) and the separate contributions from atmospheric species R(gas) (upper panels).

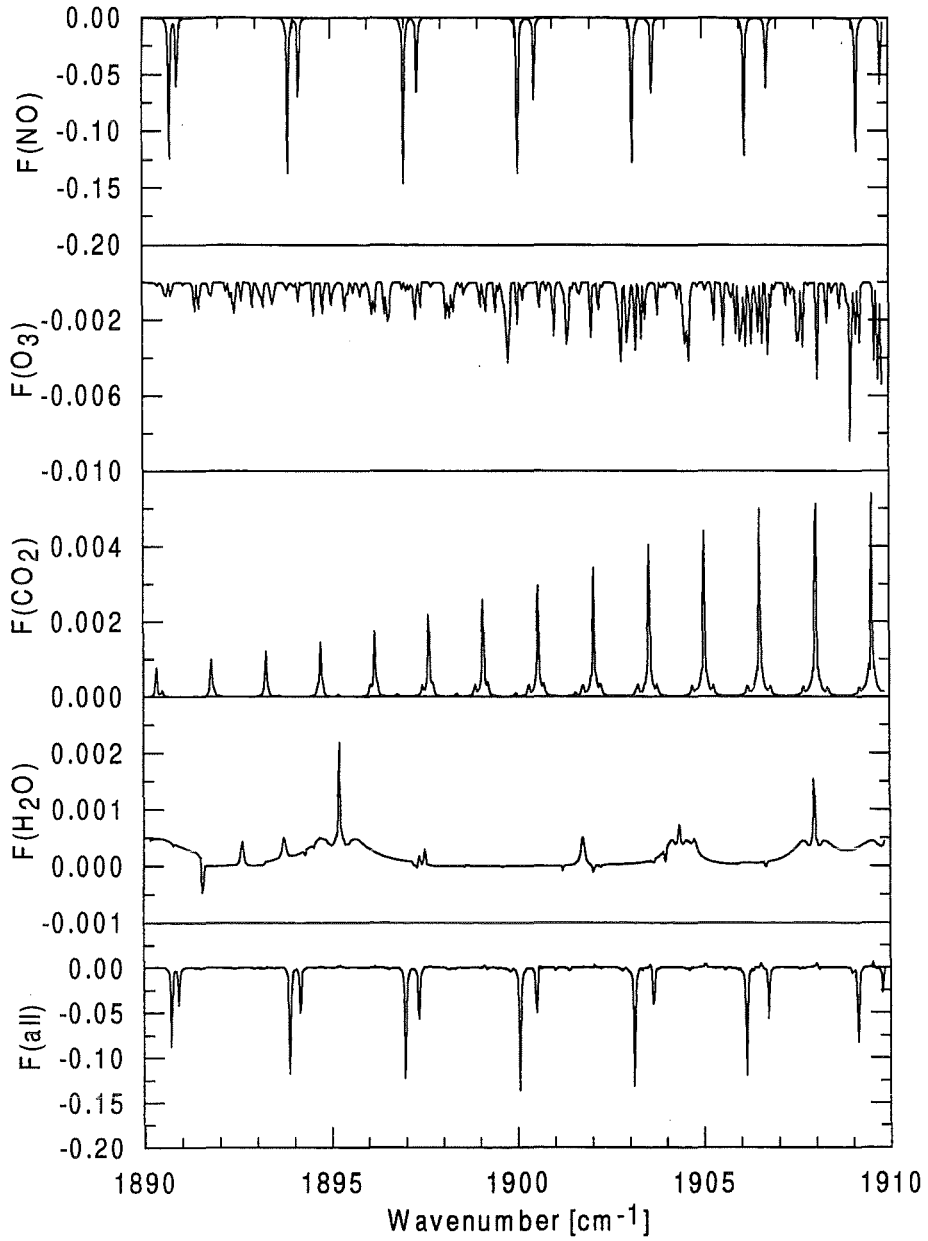

Fig. 5.10 The non-LTE effect F(all) (LTE radiance minus non-LTE one) [mW/(m^2 sr cm^{-1})] for the tangent height 10 km (lower panel) and the separate contributions from atmospheric species F(gas) (upper panels).

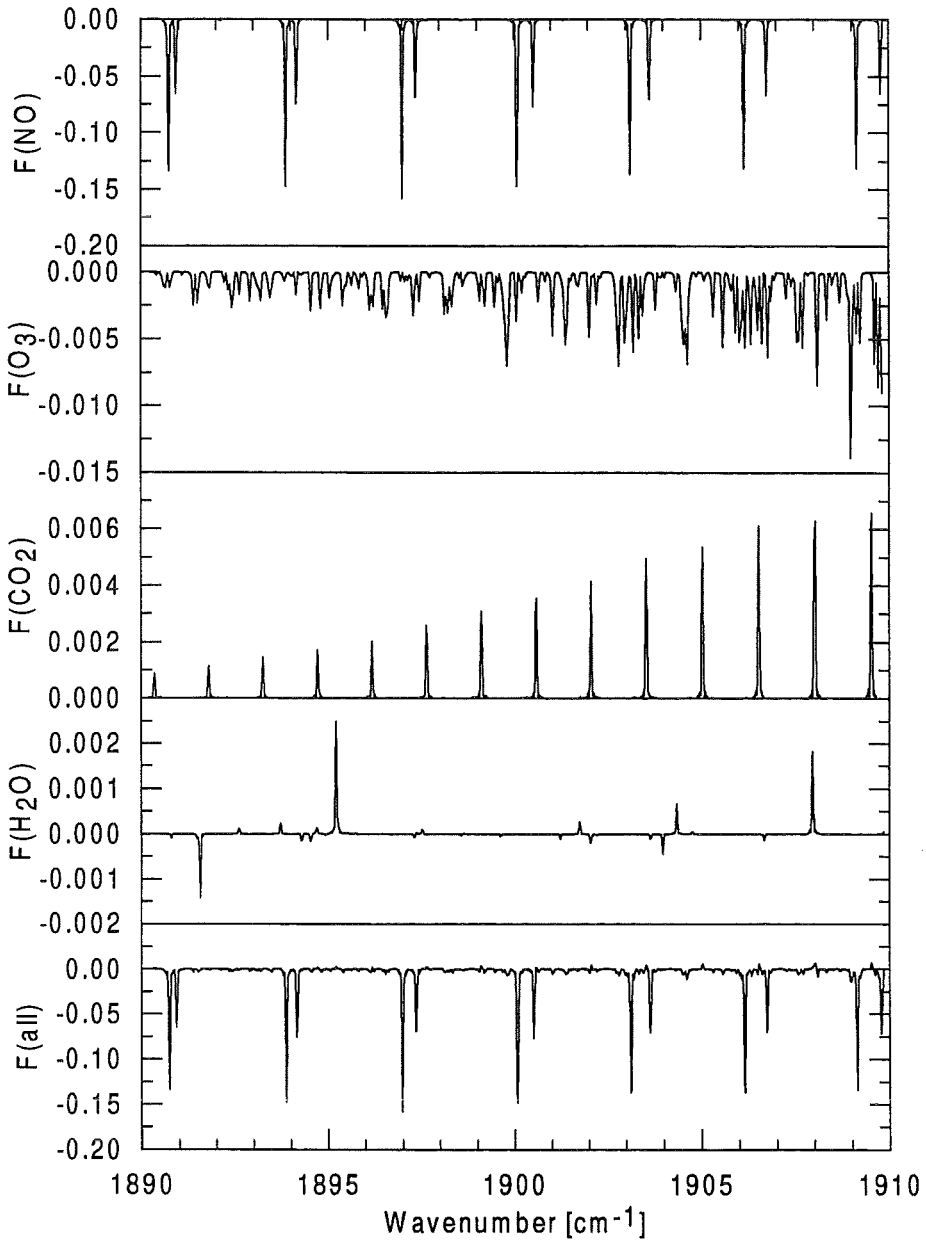

Fig. 5.11 The non-LTE effect F(all) (LTE radiance minus non-LTE one) [mW/(m^2 sr cm^{-1})] for the tangent height 30 km (lower panel) and the separate contributions from atmospheric species F(gas) (upper panels).

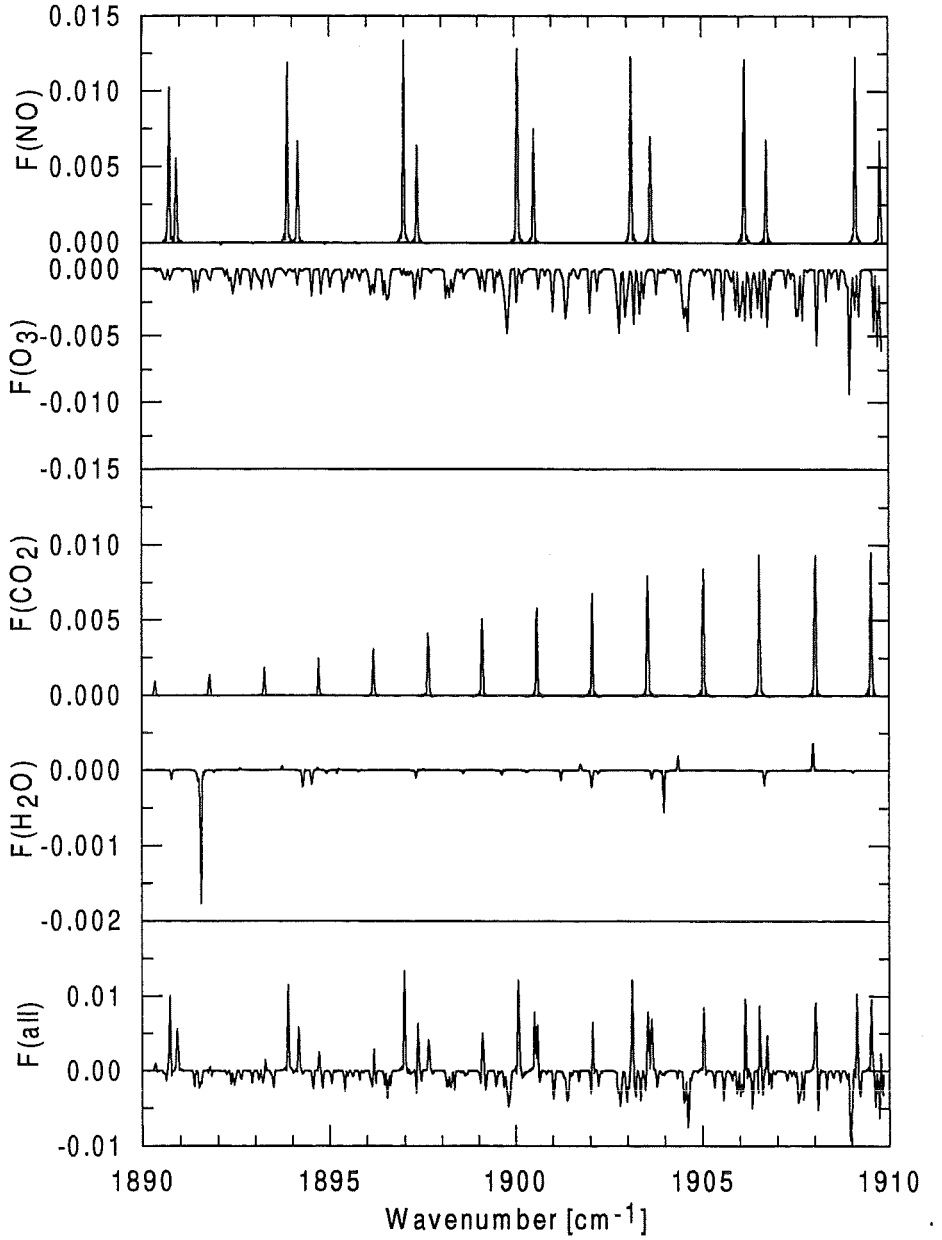

Fig. 5.12 The non-LTE effect F(all) (LTE radiance minus non-LTE one) [mW/(m^2 sr cm^{-1})] for the tangent height 50 km (lower panel) and the separate contributions from atmospheric species F(gas) (upper panels).

5.3 Non-LTE problem for the NO_2 emission.

Despite the fact that there is no non-LTE model for NO_2 at our disposal, it is important at least to locate the most intensive NO_2 bands with respect to the MIPAS measurement channels. The brief description of the vibrational bands, which are contained in HITRAN'92 spectral line database and which are relevant to the MIPAS measurement scenario, is given in the **Table 5.6**. The intensive band 010-000 is located just in the first measurement channel of MIPAS, and the other three bands (020-000, 011-010, 001-000) fall exactly in the fourth measurement channel. We stress, that the intensities of all enumerated bands are rather high. If the states are overpopulated with respect to LTE conditions, then the considerable enhancement of limb radiance can be expected. *Kerridge and Remsberg* [1989] discussed the overpopulation of states of the vibrational manifold 00v, and the non-LTE effect in the 6.2 μm region. We have no information on the deviations from LTE of the manifold 0v0 and we stress that such an information would be very important for the interpretation of measurements in the first channel and in the fourth channel as well (due to transitions 020-000 and 011-010).

There is another important problem relevant to the enhancement of radiance from the hot transitions. *Kerridge and Remsberg* [1989] discussed the importance of the contribution from the hot band non-LTE emissions. In order to simulate limb radiance spectra under non-LTE conditions, one needs not only the vibrational temperature profiles, but also the spectroscopic information (line positions, intensities, halfwidths, etc.). It should be mentioned, that HITRAN'92 database does not contain the information for the hot bands, but such information can be of great importance.

Table 5.6 NO_2 bands relevant to the MIPAS measurements.

Band center [cm^{-1}]	Transition	Wavenumber interval [cm^{-1}]	Number of lines	Sum of line intensities [cm^{-1}/molecule cm^{-2}]
749.6541	010 → 000	586 - 1001	8064	5.437E-19
1498.3461	020 → 000	1550 - 1659	464	5.3746-20
1605.4973	011 → 010	1540 - 1648	3220	1.450E-18
1616.852	001→ 000	1553 - 1698	5821	5.709E-17

6. The application of the general optimal estimation algorithm accounting for non-LTE to the problem of pressure-temperature retrievals using the CO_2 microwindows (numerical experiments).

6.1 The description of the method.

The results of the simulations of non-LTE atmospheric limb radiance described in the section 5.1 have shown that the non-LTE contribution to radiance is significant if the lines of the CO_2 laser transitions fall into the spectral microchannels, but are beyond the NESR for the lines of the CO_2 15 μm bands. The studies described below have the aim to verify this conclusion and to estimate the accuracy of the pressure-temperature (p-T) retrieval accounting for the factors other than non-LTE effect.

The outgoing radiation intensity at wavenumber ν for slant path with the tangent height z_t can be presented, in general case (taking pressure as atmospheric state parameter), as the following non-linear functional:

$$I(\nu, z_t) = F\left[T_{vi}(s), n_i(s), T(s), p(s)\right] \left\{ \begin{matrix} (i = 1,\ldots N) \\ (v = 1,\ldots M(i)) \end{matrix} \right\} \qquad \textbf{(Eq. 6.1)}$$

where T_{vi} are vibrational temperatures, n_i is the concentration of molecules, T is the kinetic temperature, p is pressure, s is the coordinate along the optical path, index "i" identifies the gas, index "v" identifies the vibrational level of the molecule of particular gas. Following the well-known approach to the formulation of inverse problems of remote sensing, we introduce the intensity corresponding to the mean state of the atmosphere, and examine its variations caused by the variations of different parameters. By making use of Taylor series expansion and after the transform from the coordinate along the optical path s to the vertical coordinate z, one can write for variations of radiance under linear approximation the following expression:

$$\mathbf{Y} = \mathbf{F}\,\mathbf{x} + \mathbf{e} \qquad \textbf{(Eq. 6.2)}$$

where **Y** is a vector composed of variations of radiance for various wavenumbers and tangent heights, **x** is the unknown total vector of the variations of the vertical profiles of atmospheric parameters:

$$\mathbf{x}=(\delta T_{vi}(z_1),\ldots,\ \delta T_{vi}(z_m),\ \delta n_i(z_1),\ldots,\ \delta n_i(z_m),\ldots)^{+} \qquad \textbf{(Eq. 6.3)}$$

Here "+" denotes transposition. The matrix **F** is formed from the values of variational derivatives of radiation intensity with respect to atmospheric parameters with corresponding quadrature coefficients, **e** is a vector of random errors of radiance measurements. The solution of the **Eq. 6.2** delivered by the regularization algorithm (often called also as the optimal estimation algorithm) can be expressed in the following form:

$$\mathbf{x} = (\mathbf{F}^{+}\Sigma^{-1}\mathbf{F} + \mathbf{D}^{-1})^{-1}\,\mathbf{F}^{+}\Sigma^{-1}\mathbf{Y} \qquad \textbf{(Eq. 6.4)}$$

where Σ is the covariance matrix of measurement random errors **e**, **D** is the a priori covariance matrix of atmospheric parameters (the diagonal elements of this matrix are squared a priori uncertainties of the atmospheric parameters in the atmospheric layers). The inversed covariance matrix D^{-1} plays a role of a regularizator. The optimal estimation algorithm makes it possible to calculate the error covariance matrix **K** of the solution **x**:

$$\mathbf{K} = (\mathbf{F}^{+}\Sigma^{-1}\mathbf{F} + \mathbf{D}^{-1})^{-1} \qquad \textbf{(Eq. 6.5)}$$

The diagonal elements of the matrix **K** characterize in this case *a posterior* uncertainty (retrieval error) of atmospheric parameters at various height levels in the atmosphere.

For the case of multi-parameter retrievals, especially when the vibrational temperature profiles are included in the set of unknowns, the determination of *a priori* covariance matrix **D** becomes rather problematic since there are practically no experimental statistical data on the vibrational temperature profiles. In order to overcome this difficulty, one can use the covariance matrix of the model form. In our calculations we used modeled covariance matrix, describing the covariances which exponentially decrease with the increase of distance between altitude levels. The joint covariance matrix is formed of blocks corresponding to every considered parameter. For the specific parameter we assumed for the covariance matrix elements the following model approximation:

$$D_{ij} = \delta x_i \, \delta x_j \exp\left(|z_j - z_j| / r_c\right) \qquad \textbf{(Eq. 6.6)}$$

where δx_i and δx_j are the a priori uncertainties of the parameter at the altitudes z_i and z_j, r_c is the radius of covariance.

The detailed description of the application of the optimal estimation method to the problem of the remote sensing of the non-LTE atmosphere can be found in the paper by *Kostsov et al.* [1992b] and *Timofeyev et al.* [1995]. The second mentioned paper contains also the description of the modeled *a priori* covariance matrix which we used in our calculations.

Finally, we pass to the consideration of the iteration procedure incorporated into the retrieval scheme. The process of linearization of the radiative transfer equation stipulates additional errors which can exceed the random errors of measurements in case the latter are small or in case the deviations of the "true" profiles from the "mean" profiles are large. In order to suppress these errors, the solution of the **Eq. 6.2** can be obtained in the iteration procedure. At every step the variational derivatives of limb radiance are recalculated for the profiles of atmospheric parameters which are obtained at the preceding step. The iteration formula can be written as follows:

$$\mathbf{x}_{i+1} = (\mathbf{F}^{+}\Sigma^{-1}\mathbf{F} + \mathbf{D}^{-1})^{-1}\,\mathbf{F}^{+}\Sigma^{-1}\,(I_m - I_c + \mathbf{F}\mathbf{x}_i) \qquad \textbf{(Eq. 6.7)}$$

where the elements of operator **F** are calculated accounting for $\mathbf{x}_i$ values, I_m is a vector composed of the limb radiance measurements, I_c is a vector composed of limb radiance values calculated on the basis of the results of the preceding iteration - x_i (see [*Timofeyev et al., 1986*]). We emphasize that though the matrix **F** changes from step to step, the error estimations (matrix **K**) are practically insensitive to that. Therefore, below we shall present the results of the error estimations based on the matrix **K** with no references to the iteration procedure.

6.2 The results of numerical experiments.

The following rigorous estimations of the retrieval accuracy have been made on the basis of the calculation of error matrix (**Eq. 6.5**).

Figure 6.1 presents the estimated retrieval accuracy for pressure σ_p, kinetic temperature σ_T, and three vibrational temperatures of the states 01101, 02201, 03301 of the CO_2 molecule: σ_1, σ_2, σ_3 correspondingly. The measurements have been simulated in the spectral range, where the first 30 preselected microwindows are located (see *Clarmann et al.* [1994]), with the spectral resolution 0.05 cm^{-1} and NESR=0.58 $mW/(m^2\ sr\ cm^{-1})$. We did not take into account sources of errors other than non-correlated noise of the detector. The tangent height step was taken equal to 2.5 km. A priori uncertainty of the pressure profile was assumed to be 15%, of the kinetic and all vibrational temperature profiles - 30 K in the entire altitude region. The results show

that the value of σ_p is better than 10% below 60-65 km and the value of σ_T is better than 10 K below 60 km. One very important note has to be made. When analyzing σ_T and $\sigma_{1,2,3}$ it should be taken into account that in the case under the discussion the non-LTE was assumed to be possible already above 30 km. In reality, since non-LTE starts from about 75-80 km, $\sigma_{1,2,3}$ in fact characterize the accuracy of the retrieval of kinetic temperature below 75-80 km. Therefore, the accuracy of the kinetic temperature retrieval is better than 3 K below 50 km, and better than 10 K up to 70 km. Above this altitude, the accuracy estimations must be treated separately.

In general, when the complete non-LTE case is considered, the possible accuracies are as follows:

- Pressure can be determined with the accuracy about 5% up to 50 km and less than 10% up to 60 km (Natural variations of pressure can reach the values of 25-50% at these altitudes.). σ_T is better than 2 K up to 40 km, better than 3 K up to 50 km, and better than 10 K up to 70 km.
- Vibrational temperature $T_v(01101)$ can be retrieved with the errors less than 20 K up to 100km. The low retrieval accuracy for the vibrational temperatures in the upper layers is the evidence of a very small influence of non-LTE on the p-T retrievals.

Since the results obtained and discussed in **section 5.1** show that in the spectral region where the preselected microwindows of the CO_2 15 μm band are located the non-LTE effects can be neglected, the next accuracy estimations have been made for the case when complete LTE is assumed in the entire atmosphere. The σ_p and σ_T for this case are shown in the **Figure 6.2** for joint p-T retrieval and separate p- and T-retrievals. The results have been obtained for the

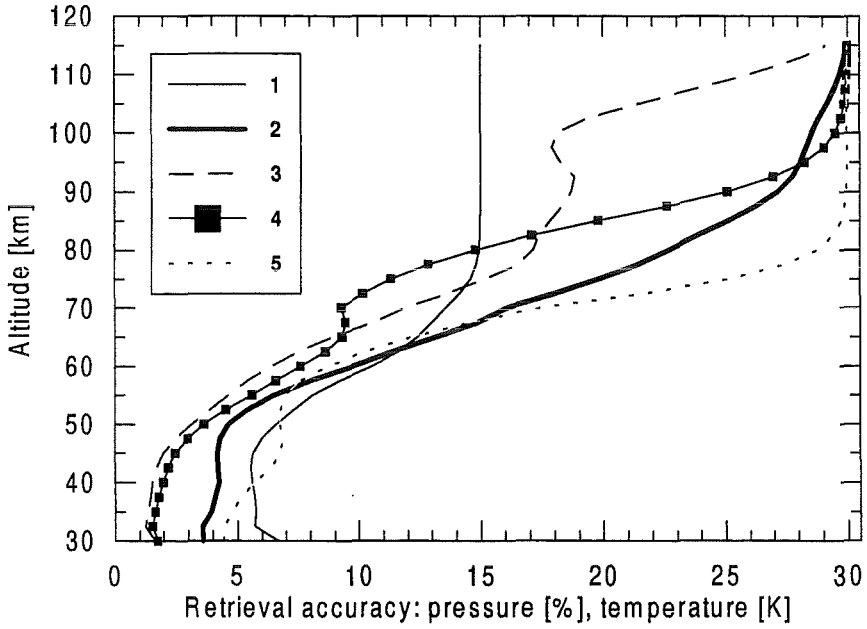

Fig. 6.1 The retrieval accuracy for pressure, kinetic temperature, and three vibrational temperatures of CO_2 estimated on the basis of the calculation of error matrix. Measurements have been simulated in the spectral region, where first 30 preselected microwindows are located, with the resolution 0.05 cm^{-1} and NESR=0.58 $mW/(m^2\ sr\ cm^{-1})$. The tangent heights were taken from 30 to 110 km with a step of 2.5 km. The non-LTE case has been considered.

1 - σ_p, retrieval accuracy for pressure;
2 - σ_T, retrieval accuracy for kinetic temperature;
3 - σ_1, retrieval accuracy for vibrational temperature $T_v(01101)$;
4 - σ_2, retrieval accuracy for vibrational temperature $T_v(02201)$;
5 - σ_3, retrieval accuracy for vibrational temperature $T_v(03301)$;

NESR value of 0.58 mW/(m^2 sr cm^{-1}), but two curves (see the Figure caption) correspond to the lower value of NESR=0.15 mW/(m^2 sr cm^{-1}).

In the case of complete LTE treatment, σ_p has the value of 5% (30-50 km) and is lower than in the case of complete non-LTE treatment especially in the area 50-65 km. σ_T is considerably lower than $\sigma_{T,1,2,3}$ in the entire height region. Such improvement is a consequence of a fewer number of unknowns in case of complete LTE treatment. When T(z) is known and p-retrieval only is performed, σ_p is about 2% up to 50 km. The known p(z) profile in the T-retrieval improves σ_T slightly only up to 55 km. The considerable improvement of accuracies can be achieved when NESR is low even for the joint p-T retrieval, as it can be seen from the figure: for example the precision of temperature retrieval is better than 5 K up to 80 km.

So the general conclusion can be made that for the altitude range of interest (up to 70 km, where LTE is valid) the kinetic temperature can be retrieved with the accuracy 1-2 K up to 50 km and with the accuracy 2-7 K in the region 50-70 km. The pressure profile can be retrieved with the accuracy 5% up to 50 km and with the accuracy 5-12% in the region 50-70 km.

In order to test the estimations of the retrieval accuracy made on the basis of the error matrix calculations, the numerical experiment on the joint p-T retrieval has been performed. Measurements have been simulated in the spectral region containing first 30 preselected

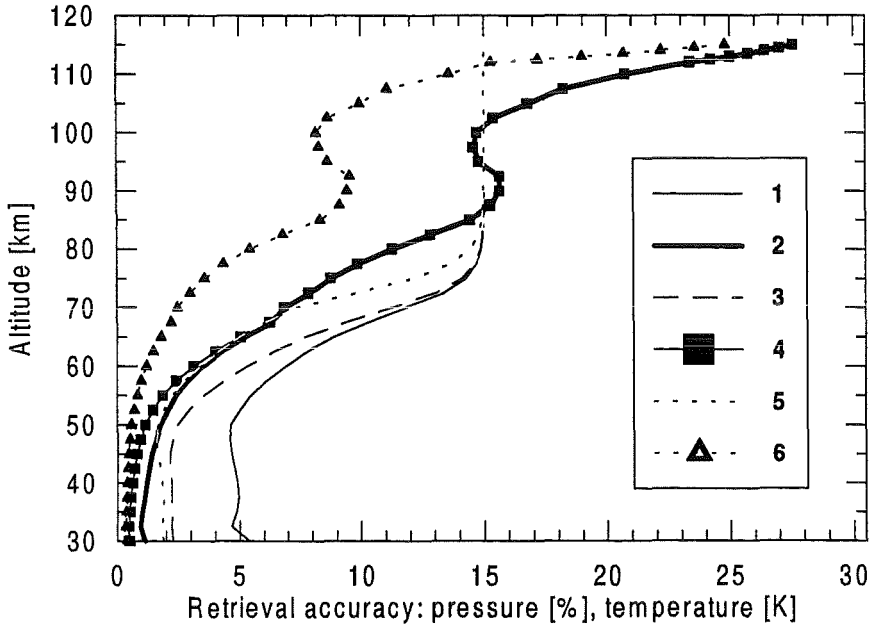

Fig. 6.2 The retrieval accuracy for pressure, and kinetic temperature, estimated on the basis of the calculation of error matrix. Measurements have been simulated in the spectral region containing first 30 preselected microwindows with the resolution 0.05 cm^{-1} and NESR=0.58 mW/(m^2 sr cm^{-1}). The tangent heights were taken from 30 to 110 km with a step of 2.5 km. The case of complete LTE has been considered. The evaluations have been done for the joint p-T retrieval and for the separate p- and T-retrievals.

1 - σ_p, retrieval accuracy for pressure, p-T retrieval;
2 - σ_T, retrieval accuracy for kinetic temperature, p-T retrieval;
3 - σ_p, retrieval accuracy for pressure, p-retrieval only;
4 - σ_T, retrieval accuracy for temperature, T-retrieval only;
5 - σ_p, retrieval accuracy for pressure, p-T retrieval, low NESR;
6 - σ_T, retrieval accuracy for temperature, p-T retrieval, low NESR;

microwindows with the resolution 0.05 cm^{-1} and NESR=0.58 $mW/(m^2\ sr\ cm^{-1})$. The atmospheric radiance was calculated assuming the real non-LTE conditions, but the inverse problem was solved as if the complete LTE was valid. The errors due to non-linearity of the approximation of the radiative transfer operator **A** were corrected in the iteration procedure.

It should be mentioned that measured spectrum has been simulated for the atmospheric model, where not only non-LTE features were present but also the variations of the number density of the absorbers. This atmospheric model will be referred below as "real" or "true" atmosphere. The mean profiles of atmospheric parameters have been varied in the way as it is shown in **Table 6.1**. Variations of atmospheric parameters have been selected to a certain extent arbitrarily - in particular case with the change of their sign in order to investigate the possibilities of retrieval of the variations of such kind.

Table 6.1 Modeling of the variations of atmospheric parameter profiles. (Within the height range 30-115 km relative variations have been interpolated linearly.)

Parameter	Variation at 30 km	Variation at 115 km
Pressure	10%	10%
Kinetic and all vibrational temperatures	10% (~23 K)	-15% (~40 K)
H_2O	30%	-30%
O_3	30%	-30%
CO_2	5%	-5%

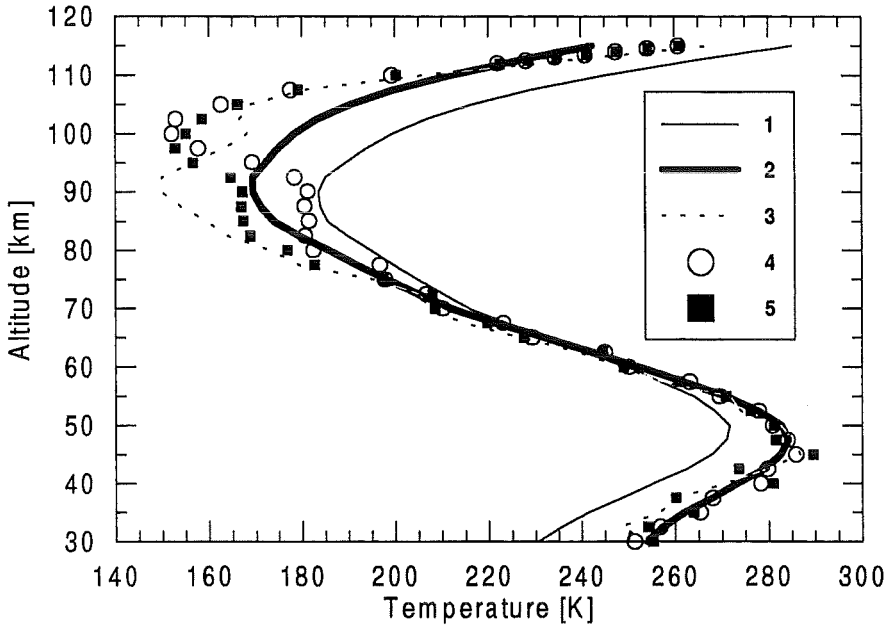

Fig. 6.3 The results of temperature profile retrieval in the numerical experiment for joint p-T retrieval. The inverse problem has been formulated for the LTE conditions in the entire atmosphere, but measurements have been simulated accounting for non-LTE. The iteration process was performed in order to eliminate the errors caused by linearization of the radiative transfer operator.

1 - mean profile;
2 - "true" profile;
3 - retrieved on the 1st iteration;
4 - retrieved on the 2nd iteration;
5 - retrieved on the 3rd iteration.

The kinetic temperature profiles retrieved in the numerical experiment which correspond to consecutive iterations are shown in **Figure 6.3**. (The convergence criterion was the stabilization of the solution in combination with the fitting of the "real" spectrum within the frames of NESR.) The satisfactory results of the retrieval can be seen up to the altitude 90 km. However, the retrieved profiles, especially on the 1st and 3rd iterations display oscillations in the altitude region 30-50 km. These oscillations are clearly visible in **Figure 6.4** where the results of the temperature profile reconstruction are shown in terms of absolute retrieval error (left panel). The absolute retrieval errors oscillate in the region 30-50 km from positive to negative values and exceed the theoretically estimated a posterior uncertainty in the kinetic temperature profile. The oscillations can be observed also above 50 km, but they are within the "corridor" of a posterior uncertainty.

The reconstructed pressure profiles have not been plotted since the "real" profile deviated from the mean one only by 10% and these deviations could not be clearly distinguished neither with linear nor with logarithmic scaling. The results of the retrievals of pressure are plotted in **Figure 6.4** (right panel) in terms of relative retrieval errors. At the 1st iteration, the pressure profile was reconstructed with enormously large errors up to 70% in the vicinity of 35 km and up to 40% in the vicinity of 65-70 km. The following iterations yielded the considerable reduction of errors, which remain, however, too large in the height region 30-50 km, where they are oscillating and exceeding the a posterior value of the uncertainty of pressure profile.

The results display the convergence already after the 2nd iteration because the rms discrepancy in spectra approached the value of NESR of measurements. After the 3rd iteration, rms discrepancy in spectra remained stable, but the maximal absolute discrepancy decreased by a factor of 2. Though the convergence was achieved already after the 2nd iteration (in terms of

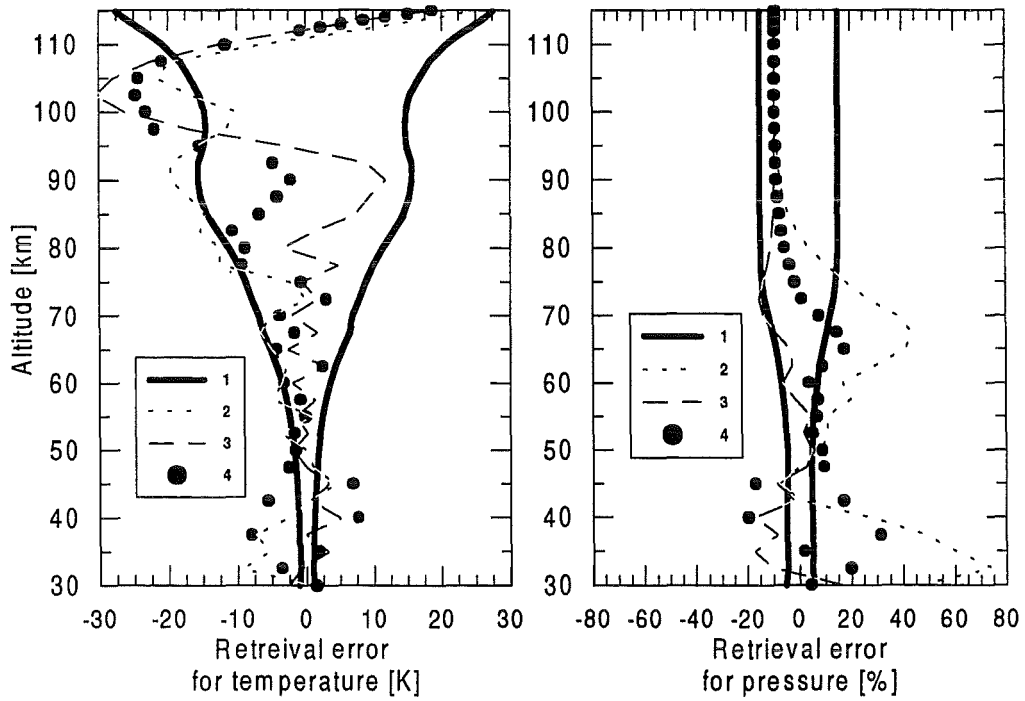

Fig. 6.4 The results of pressure-temperature retrieval in the numerical experiment in terms of retrieval errors. The inverse problem has been formulated for the LTE conditions in the entire atmosphere, but measurements have been simulated accounting for non-LTE and possible variations of gas profiles.

1 - a priori uncertainty;
2- results of the 1st iteration;
3 - results of the 2nd iteration;
4 - results of the 3rd iteration.

discrepancy between spectra), the 4th iteration has been made in order to investigate the behavior of oscillations of the retrieval errors. The results have shown, that profiles reconstructed in the 4th iteration do not differ noticeably from ones in the 3rd iteration, and the oscillation remained. The attempt has been made to perform the retrievals taking the value of the correlation radius for pressure and temperature of 10 km in order to smooth profiles (in all other cases it was assumed to be 5 km). But the obtained results displayed oscillations even in the case of strong correlations between different atmospheric layers.

The general conclusion which follows from the described retrievals is the following:
- the reconstruction of the kinetic temperature profile displays oscillations;
- the retrieval errors for the pressure profile display rather large oscillations, and the reconstruction of the profile is not good.
- the iteration procedure converged after the 2nd iteration.

So, the supplementary investigations were necessary to find the explanation for the oscillations in the reconstructed profiles.

In order to investigate whether oscillations are stipulated by the non-LTE contribution to limb radiance which can exceed NESR in the centers of the strongest lines in the preselected microwindows and which was not accounted for in the previous LTE task, the numerical experiment was performed with the correct procedure aimed to reconstruct the total set of unknown variables: pressure, kinetic temperature, concentrations of absorbers (CO_2, H_2O, O_3) and the vibrational temperatures for CO_2 and O_3. It was assumed that all parameters except p(z) and T(z) are so-called "interfering parameters". For these interfering parameters no high accuracy was expected because of the lack of information in the spectrum, but still these parameters should be accounted for in the retrieval, because their total contribution to the variations of radiance can be noticeable with respect to NESR.

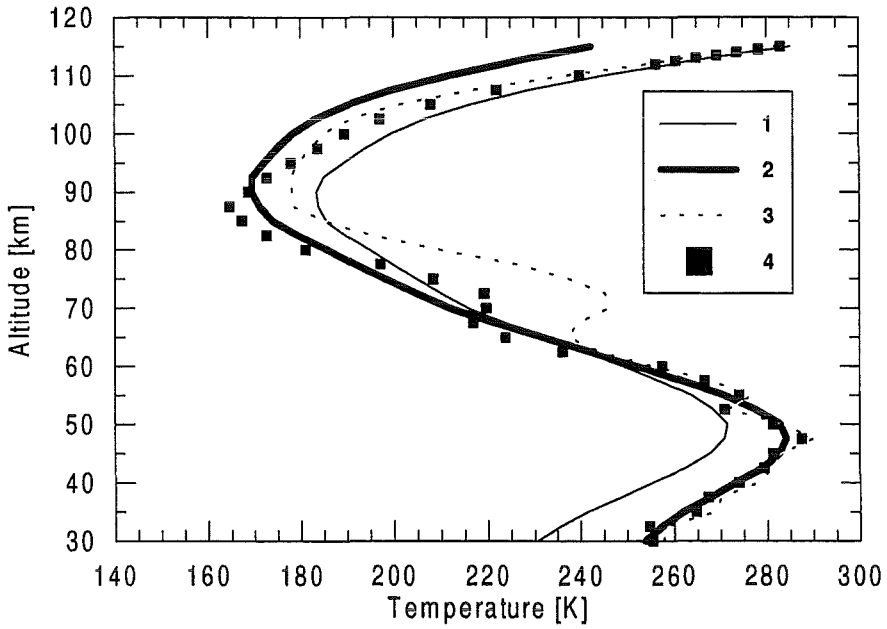

Fig. 6.5 The results of temperature profile retrieval in the numerical experiment for joint p-T retrieval. The inverse problem has been formulated for the non-LTE conditions in the entire atmosphere accounting also for the variations of the gas concentration.
1 - mean profile;
2 - "true" profile;
3 - retrieved on the 1st iteration;
4 - retrieved on the 3rd iteration;

The results of the reconstruction T(z) and the retrieval errors for this case are presented in **Figures 6.5** and **6.6** (for the 1st and the 3rd iterations), which are similar to the **Figures 6.3** and **6.4**. As it can be seen from **Figures 6.5** and **6.6**, the oscillations of the retrieval errors became much smaller and they are within the corridor of a posterior uncertainty. In the height region 30-50 km the retrieval of pressure and temperature in the complete non-LTE task is much better than in the LTE task. The results show also that the iteration procedure converged after the 2nd iteration with respect to the discrepancy between spectra (the rms discrepancy approached the value of NESR). The results obtained for the complete non-LTE task indicate therefore that the possible reason for the unexpected oscillations of the retrieval errors in the LTE task may be caused by the influence of non-LTE or by the uncertainties of the number density of the absorbers.

The main objective of the additional calculations described further in this section is the investigation of the origin of the oscillations of the retrieved temperature and pressure profiles in case when the inverse problem was solved assuming LTE conditions in the entire atmosphere and the spectrum was calculated accounting for non-LTE.

In order to estimate the influence of different parameters on the p-T retrieval several tasks were set on the run. In these tasks different profiles were set known and unknown. "Known" means that the real profile is equal to the mean one and "unknown" means that real profile differs from the mean profile (initial guess) due to variations indicated above. The following table contains the description of the tasks and the results obtained in terms of the presence of oscillations (we stress that the retrievals in all tasks were performed for the same spectral region containing 30 preselected microwindows and for the same value of NESR=0.58 mW/(m^2 sr cm^{-1})):

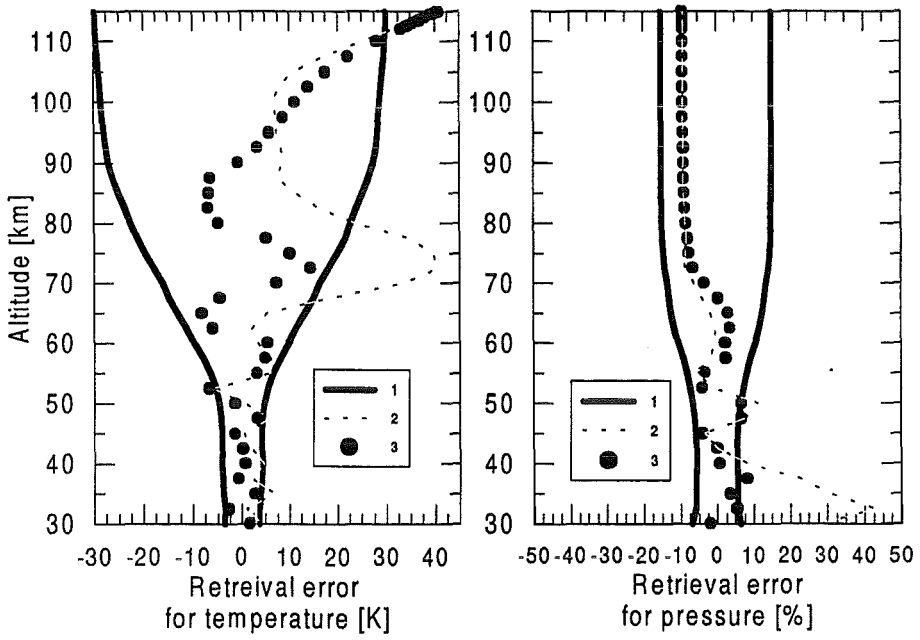

Fig. 6.6 The results of pressure-temperature retrieval in the numerical experiment in terms of retrieval errors. The inverse problem has been formulated for the non-LTE conditions in the entire atmosphere, and measurements have been simulated accounting for non-LTE and possible variations of gas profiles.

1 - a priori uncertainty;
2- results of the 1st iteration;
3 - results of the 3rd iteration;

Table 6.2 The description of tasks (numerical experiments).

Task	Non-LTE	H_2O	O_3	CO_2	Oscillations
0	No	known	known	known	No
1	Yes	known	known	known	No
2	Yes	unknown	unknown	known	Yes
3	Yes	known	unknown	known	Yes
4	Yes	unknown	known	known	No

The obtained results indicate that:
- non-LTE does not stipulate oscillations (task 1);
- ozone is the main interfering parameter (when it is set as unknown), which causes oscillations (task 3). However we stress, that we simulated measurements not exactly within the boundaries of preselected microwindows, but in a wider spectral ranges. So this result is the evidence of the necessity to avoid ozone interference in the microwindows, what actually was done by the preselection.

The first conclusion can be made that non-LTE has no influence on the retrieval of temperature and pressure profiles up to 80 km if measurements in specific preselected microwindows are used for the retrieval.

The second conclusion can be made that the uncertainties in the ozone profile can severely influence the p-T retrievals in the area of preselected microwindows in the altitude range 30-50 km. For the estimation of the ozone interference, the calculations of limb radiance variations stipulated by variations of ozone number density have been performed in the region 686-716 cm^{-1}, where the preselected microwindows are located. The variations of ozone number density have been taken as it is indicated in **Table 6.1**. In these calculations all other parameters have been fixed and LTE conditions were assumed both for ozone and carbon dioxide. Simulated limb radiance variations for tangent heights 30 km and 40 km are shown in **Figure 6.7** (for the sake of optimal scaling we present the variations only in the spectral interval 686-696 cm^{-1}, in the interval 969-716 cm^{-1} the results display the same features). As it can be seen from the figure, limb radiance variations exceed considerably the value of NESR practically in all preselected microwindows for both tangent heights - 30 and 40 km. In this case the SNR (the ratio of limb radiance variations, stipulated by variations of ozone profile, to NESR) can reach 5 for tangent height 30 km and 2-3 for tangent height 40 km. So, when the uncertainty of ozone profile was not taken into account in the numerical experiments, the oscillations in the retrieved profiles appeared, since the interfering signal stipulated by ozone variations is rather high. Therefore it is necessary to apply a priori information on the ozone profile before performing p-T retrievals, or to solve the joint inverse problem accounting for uncertainties of ozone profile.

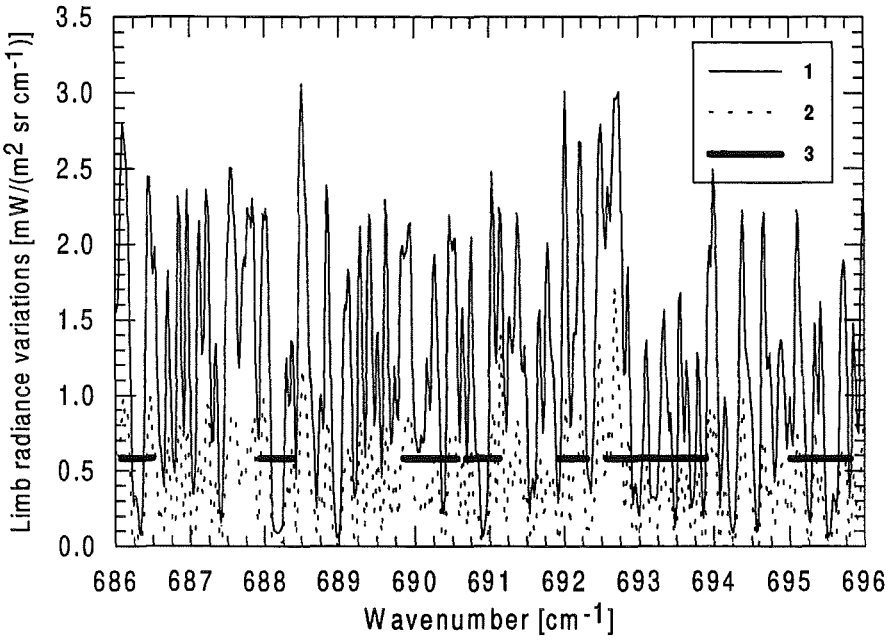

Fig. 6.7 Variations of limb radiance stipulated by variations of ozone profile. Variations of the other parameters have been set to zero. Spectral resolution 0.05 cm^{-1}. Thin solid line: tangent height 30 km. Dashed line: tangent height 40 km. The value of NESR is shown by thick lines in the areas where the preselected microwindows are located.

7. Discussion and conclusions.

The results of simulations of balloon-borne and space-borne measurements of limb radiance with account for non-LTE conditions in several spectral domains comprising the absorption bands of carbon dioxide, ozone and nitric oxide have made it possible to investigate the possibility of detecting non-LTE features from the balloon-borne platforms and to estimate numerically the possible influence of non-LTE effect on the MIPAS balloon and satellite limb radiance measurements.

The simulations of limb emission accounting for non-LTE conditions are important since the possible non-LTE effect can effect the results of the retrievals of temperature and trace gas profiles by its contribution to radiance, and the retrieval procedures in this case can provide unreal quantities (see, for example [*Kerridge and Remsberg*, 1980]). Depending on the magnitude of the non-LTE effects, one or another correcting algorithm should be applied. On the other hand, if more general approach is accepted for the retrieval procedure, there is a good possibility to study the non-LTE effects by the joint retrieval of kinetic temperature profile, trace gas profiles and the vibrational temperature profiles [*Timofeyev et al.*, 1995]. Such general approach is possible in the case of the high-accuracy and high-resolution limb emission measurements in broad spectral regions containing a number of vibrational bands (this is the very case of the MIPAS measurements). In both cases the simulations of limb emission with account for non-LTE should be performed at the first step in order to:

- investigate the necessity of a correcting algorithm;
- select the most informative spectral region if the problem of joint retrieval of atmospheric parameters (including vibrational temperatures) is to be solved.

It should be mentioned, however, that the rigorous simulation of non-LTE atmospheric radiance is a rather complicated task due to the following reasons:

- Usually, due to the overlapping of bands of different gases, which are influenced by non-LTE, it is necessary to have the non-LTE population model, which comprises all the gases optically active in the wavenumber of interest. At present, we do not have the information about such a model. Many of models have been developed focusing on one or another gas under non-LTE. Of course, one should mention the non-LTE model included in FASCOD3P computer code. This model comprises the vibrational temperatures for a number of vibrational states of several gases. However, in this model no dependence on diurnal variations of the populations of vibrational states is provided which makes the application of this model to some extent restricted.
- The calculation of vibrational state populations (vibrational temperatures) is itself rather complicated problem. Without discussing this problem in detail, we should mention, that, for example, the values of energy exchange rate coefficients are known with a limited accuracy, and sometimes the relevant information is missing. Sometimes the contribution of different mechanisms to the departure of local thermodynamic equilibrium is not perfectly known, and this obstacle also contributes to the complexity of the problem.
- The problem of the validation of non-LTE models is very important since the population distributions can be estimated only indirectly from the radiation measurements.

The MIPAS-B balloon campaigns have been reviewed from the point of the possibility to detect the non-LTE effect (day-time conditions, maximal flight altitude and tangent altitude of observations). One spectrum was chosen which corresponds to the maximal balloon height and tangent height during the 1990 campaign.

The estimation has been made of the value of non-LTE effect which could have been present in spectra. The term "non-LTE" effect has been assumed for the difference between radiances

calculated for non-LTE and LTE conditions. The spectra have been analyzed in broad and narrow spectral intervals within the range 910-1030 cm^{-1} with a resolution of 0.076 cm^{-1}. The measurement error (noise equivalent spectral radiance - NESR) was taken equal to 0.2 $mW/(m^2$ sr $cm^{-1})$. The simulations of non-LTE spectra have shown that it is impossible to detect non-LTE effects in the experimental data obtained in the MIPAS balloon campaign in 1990 due to low magnitude of these effects in the spectral interval that was measured. It was shown that for the balloon height ~40km, limb-viewing geometry and NESR=0.2 $mW/(m^2$ sr $cm^{-1})$ it would have been possible to detect non-LTE effect if the interval 990-1030 cm^{-1} had been considered. However this spectral interval was not covered by the MIPAS-B measurements available at the moment. We stress, that in reality the problem of the detection of the non-LTE effect will be more complex due to the uncertainties of the large number of atmospheric parameters.

The investigations of the magnitude of non-LTE effect which can be present in the MIPAS space-borne measurements included 15 μm and 10 μm CO_2, 9.6 μm O_3, and 5.3 μm NO absorption bands.

It was shown that the measurement accuracy 0.2 $mW/(m^2$ sr $cm^{-1})$ is high enough to detect non-LTE effects up to the altitudes of 85-90 km in space-borne measurements with the resolution of 0.076 cm^{-1}, for CO_2 lines belonging to the so-called laser band 00011-10001. We did not investigate the 9.6 μm ozone band in detail and limited calculations to the specific bands overlapping with the CO_2 laser band. For these ozone bands, the non-LTE effect exceed the NESR of MIPAS space-borne measurements.

Special attention has been paid to the estimation of the non-LTE effect in the spectral region where the microwindows preselected for the pressure-temperature retrieval are located. The results have shown, that the non-LTE effect appears to be rather small for all microwindows except those containing CO_2 lines of the laser transition.

The non-LTE effect in the 5.3 μm NO bands was investigated in the most detail. The non-LTE model for the investigation of NO non-LTE emissions was taken from FASCOD3P computer code. The literature review has shown that the non-LTE effect for nitric oxide has been studied intensively. The evidence for the vibrational non-LTE was detected by the ISAMS instrument. The CIRRIS-1A interferometer provided the indication of the rotational non-LTE at tangent heights between approximately 115 and 190 km.

The analysis of the vibrational temperature profiles from FASCOD3P computer code has shown that the non-LTE effect for the X1/2-1 and X1/2-2 states of NO starts already in the troposphere. The deviation of vibrational temperature T_v(X1/2-1) from the kinetic temperature can reach 30 K in the stratosphere and 50 K in the vicinity of the mesopause. The deviation of vibrational temperature T_v(X1/2-2) from the kinetic temperature can reach 100 K in the stratosphere and 140 K in the vicinity of the mesopause. Simulated monochromatic limb radiance profile in the center of a strong line of the fundamental vibrational transition exhibited non-LTE already for the tangent height of 1 km. The maximal non-LTE effect appeared to take place for the tangent height 30 km. The same features were obtained for a strong line of the first hot transition, however the magnitude of the non-LTE effect appeared to be lower by a factor of 60. Limb radiance profiles were simulated for the general case with line overlapping for a spectral resolution of the MIPAS measurements of 0.05 cm^{-1}. For the NO bands taken separately it was shown that the non-LTE effect in the limb radiance exceeds the NESR of the MIPAS measurements in the centers of strong lines of the fundamental transition at tangent heights between 1 km and 35 km by a factor of 5-10. The limb radiance values for the lines of the first hot transition are far beyond the level of detectability (NESR). Though the non-LTE effect for these lines is very strong (the non-LTE contribution in radiance is dominant), it is not possible to detect it in the MIPAS measurements.

The simulations of limb radiance spectra were performed also for the real case, accounting (additionally to NO) for the major atmospheric constituents: H_2O, CO_2, O_3. The non-LTE models for these gases were taken also from FASCOD3P computer code. It was shown that in the spectral region, where the most intensive NO lines are located, the limb radiance is determined mainly by H_2O, CO_2 and NO. The emission from ozone bands is practically negligible. Despite the fact that the emission from water vapor and carbon dioxide is very strong, the non-LTE effect originating from these constituents is beyond the level of detectability (NESR of MIPAS) for all tangent altitudes considered (10 km, 30 km, 50 km). Such low values of the non-LTE effect are due to the absence of the strong lines in the spectral region of interest. However, the emission from NO is clearly "visible" on the background of the strong emissions from water vapor and carbon dioxide.

On the basis of the simulations of non-LTE limb radiance profiles and spectra in the spectral region of NO bands, one can derive the following main conclusion: the non-LTE effect should be taken into account for the NO fundamental vibrational transition while interpreting the MIPAS limb measurements for the tangent heights up to approximately 50 km.

The evidence for non-LTE effect in the emission from NO_2 was obtained indirectly during the interpretation of LIMS measurements. Several anomalous features of spectra could have been explained only by the considerable enhancement of limb radiance by the emission from NO_2 due to non-LTE. The literature review, unfortunately, did not provide the information on the non-equilibrium populations of the NO_2 vibrational states. As far as the non-LTE problem of NO_2 is concerned relative to the MIPAS measurements, due to the absence of the non-LTE model it was impossible to perform the estimations of the influence of non-LTE effect on limb measurements. In the discussion of the problem, three important items were stressed:

- there could be possible non-LTE influence in the first and in the fourth measurement channels;
- in order to study the non-LTE contribution to limb radiance in the MIPAS channels, the non-LTE model is necessary, which comprises vibrational manifolds 0v0 and 00v;
- there is a lack of spectroscopic information on the hot bands of NO_2 in the HITRAN'92 database.

In the present study the possible influence of the non-LTE effects on the pressure-temperature retrieval from limb radiance measurements to be performed by MIPAS was investigated. Calculations of LTE and non-LTE limb radiances have been performed in the centers of several lines falling in the preselected microwindows in the region of CO_2 15 μm bands. The results have shown that in the centers of the strong lines corresponding to the laser band the non-LTE contribution can exceed NESR even for the tangent altitudes of 30-50 km. Though the atmosphere is under LTE at these altitudes, the non-LTE contribution comes from the higher layers, which are under non-LTE.

The numerical experiments were performed using the optimal estimation method (the method of statistical regularization) aimed to reconstruct pressure and temperature profiles. Two basic tasks were considered:

1) measurements were simulated correctly accounting for non-LTE, but the retrieval procedure was organized assuming LTE in the entire atmosphere;
2) measurements were simulated correctly accounting for non-LTE, and the retrieval procedure was organized correspondingly accounting for all unknown variables (pressure, temperature, concentration of absorbers, all vibrational temperatures considered in the study). In this task the main attention, however was paid to the reconstruction of pressure and temperature.

The results of the reconstruction of pressure and temperature profiles have shown the advantages of the second approach where the obtained profiles displayed better accuracy and

while in the first task the considerably larger oscillations of the profiles and more lower retrieval accuracy was observed. The investigation of separate influence of non-LTE effects and the uncertainties in the number density profiles of absorbers has shown, however, that non-LTE effects does not influence p-T retrieval in the altitude range 30-50 km. The investigation of separate influence of the uncertainties in the number density profiles of specific absorbers has shown that the uncertainty in ozone number density can influence severely the results of p-T retrieval in the altitude range 30-50 km. However we stress, that we simulated measurements not exactly within the boundaries of preselected microwindows, but in a wider spectral ranges. So this result is the evidence of the necessity to avoid ozone interference in the microwindows, what actually was done by the preselection. If ozone profile is known, than the retrieval of temperature profile in height range 30-50 km is possible with the accuracy better than 2 K and the retrieval of pressure profile in the same height range is possible with the accuracy better than 5% despite the fact that non-LTE is not accounted for. These accuracy estimations hold true for the value of NESR of 0.58 mW/(m^2 sr cm^{-1}). It should be stressed, that these conclusions are valid if the preselected microwindows are utilized for the retrieval procedure. For other spectral regions the specific investigations should be carried out.

We stress that the accuracy of obtained estimations can be increased if we have other non-LTE models at our disposal (vibrational temperature distributions), or high-accuracy and high-resolution limb emission measurements in the spectral regions of interest. In the first case, there would be a possibility to make estimations of the variations of non-LTE effect (diurnal, spatial, seasonal). In the case of availability of limb measurement in the spectral regions of interest, there would be a possibility to solve the inverse problem of the joint retrieval of kinetic temperature profile, trace gas vertical distribution and the vibrational temperature profiles and to compare the results with the theoretical predictions.

8. Recommendations.

On the basis of the presented study, finally, we outline several recommendations for the further investigations of the non-LTE effect in connection with the future space measurements by the MIPAS instrument:

1. The expanding of the list of the considered gases and absorption bands (non-LTE) for the MIPAS channels.
2. More general and rigorous formulation of the problem of pressure-temperature retrievals. The search for the optimal combination of spectral intervals.
3. The development of the algorithms for simple non-LTE effect correction in the process of measurement interpretation.
4. The detailed analysis of the retrieval of vibrational temperatures from the MIPAS measurements.
5. The interpretation of the recent balloon-borne MIPAS measurements.
6. The development of the specialized software for non-LTE correction and non-LTE inverse problems.

9. Acknowledgments.

The authors are grateful to A.A.Kutepov and M.Lopez-Puertas for the data on vibrational temperatures for CO_2 and to R.O.Manuilova for the data on vibrational temperatures for O_3.

This work was performed in the frame of the Cooperation Agreement for 1993-1995 between the Institut für Meteorologie und Klimaforschung (Forschungszentrum Karlsruhe, Germany) and the Research Institute of Physics (St.Petersburg State University, Russia).

10. References.

Anderson G.P. et al., 1986:

G.P.Anderson, S.A.Clough, F.X.Kneizys, J.H.Chetwynd, E.P.Shettle. AFGL Atmospheric Constituent Profiles (0-120km). AFGL-TR-86-0110, *Environmental research papers*, No 954, 1986, 43p.

Ballard J. et al., 1993:

J.Ballard, B.J.Kerridge, P.E.Morris, and F.W.Taylor. Observations of V=1-0 emission from thermospheric nitric oxide by ISAMS. *Geophysical Research Letters*, Vol. 20, No 12, pp. 1311-1314, June 18, 1993.

Caledonia G.E. and Kennealy J.P., 1982:

NO infrared emission in the upper atmosphere. *Planet. Space Sci.*, Vol. 30, p. 1043, 1982.

Clarmann T.v. et al., 1994:

T.v.Clarmann, A.Linden, H.Oelhaf. The simultaneous retrieval of pressure and temperature from MIPAS limb emission spectra. *Final Report. March 1994. ESA Purchase Order No 131253*, 91p.

Degges T.C., 1971:

Vibrationally excited nitric oxide in the upper atmosphere. *Applied Optics*, Vol. 10, No 8, pp. 1856-1860, 1971.

Dem'yanikov A.I. and Kutepov A.A., 1987:

The possibility for remote thermal sounding of upper atmospheric layers on slant paths accounting for deviations from local thermodynamic equilibrium. *Atmospheric and Oceanic Physics*, Vol. 23, No 5, pp.510-518 (in Russian edition), 1987.

Dem'yanikov A.I. and Kutepov A.A., 1988:

The possibility for determining the quantum survival probability in the 15 μm CO_2 band based on remote sounding data. *Atmospheric and Oceanic Physics*, Vol. 24, No 4, pp.387-393 (in Russian edition), 1988.

Fichet P. et al., 1992:

P.Fichet, J.R.Jevais, C.Camy-Peyret, and J.M.Flaud. NLTE processes in ozone: importance of O and O_3 densities near the mesopause. *Planet. Space Sci.*, Vol. 40, pp. 989-1009, 1992.

Green B.D. et al., 1986:

B.D.Green, W.T.Rawlins, and R.M.Nadile. Diurnal variability of vibrationally excited mesospheric ozone as observed during the SPIRE mission. *J.Geoph. Res.*, Vol. 91, pp. 311-320, 1986.

Hollweg et al., 1995:

H.-D.Hollweg, V.S.Kostsov, G.Schlüssel, P.Schlüssel, Yu.M.Timofeyev, M.V.Tonkov, A.V.Polyakov, N.N.Filippov. Interaction at mm and Optical Frequencies. Part II: Specific Atmospheric Absorption and Emission Features: Investigation and Modeling. Final Report. ESA ESTEC Contract No. 10603/93/NL/NB. Zentrum für Meeres- und Klimaforschung der Universität Hamburg, Meteorologisches Institut, 1995.

Ishov et al., 1995:

A.G.Ishov, A.A.Kutepov, and H.Oelhaf. On the possibility of retrieving non-LTE ro-vibrational populations of CO_2 molecules and kinetic temperature from high resolution limb radiance measurements in the IR CO_2 bands. IUGG XXI General Assembly in Boulder, Colorado. July 2-14, 1995.

Kaye J.A. and Kumer J.B., 1987:

Nonlocal thermodynamic equilibrium effects in stratospheric NO and implications for infrared remote sensing. *Applied Optics*, Vol. 26, No 22, pp. 4747-4754, November 15, 1987.

Kerridge B.J. and Remsberg E.E., 1989:

Evidence from the limb infrared monitor of the stratosphere for nonlocal thermodynamic equilibrium in the ν_2 mode of mesospheric water vapor and the ν_3 mode of stratospheric nitrogen dioxide. *Journal of Geophysical Research*, Vol. 94, No D13, pp. 16323-16342, November 20, 1989.

Kockarts G., 1980:

Nitric oxide cooling in the terrestrial thermosphere. *Geophysical Research Letters*, Vol. 7, No 2, pp. 137-140, February 1980.

Kostsov V.S. et al., 1992a:

V.S.Kostsov, V.V.Rozanov, Yu.M.Timofeyev, H.Grassl, and A.A.Kutepov. The spectral structure of the nonequilibrium outgoing limb radiance in the 15 μm CO_2 absorption band. *Atmospheric and. Oceanic Physics*, Vol. 28, No 3, pp. 214-222 (in English edition), 1992.

Kostsov V.S. et al., 1992b:

V.S.Kostsov, Yu.M.Timofeyev, and H.Grassl. Possibilities of determining vibrational temperature profiles of 15-μm CO_2 band from Earth limb radiation measurements. *Atmospheric and. Oceanic Physics*, Vol. 28, No 6, pp. 457-465 (in English edition), 1992.

Kostsov V.S. et al., 1995:

V.S.Kostsov, Yu.M.Timofeyev, and H.Grassl. On the accuracy of the limb sounding of the atmosphere in the 10.4 μm, 15 μm CO_2 and 9.6 μm O_3 bands with account for non-LTE. *Adv. Space Res.*, Vol. 16, No 10, pp.(10)87-(10)90, 1995.

Kutepov A.A. and Shved G.M., 1978:

Radiative transfer in the 15-μm CO_2 band with the breakdown of local thermodynamic equilibrium in the Earth's atmosphere. *Atmos. Ocean. Phys.*, Vol.14, pp. 18-30, 1978.

Kutepov A.A. et al., 1993:

Non-LTE radiative transfer in the 4.7 μm band of CO: vibration-rotational non-LTE and its effects on limb radiance. In: *"IRS'92: Current problems in atmospheric radiation"*, S.Keevallik and O.Kärner (Eds), A.Deepak Publishing, pp. 548-551, 1993.

Lopez-Puertas M. et al., 1986a:

M.Lopez-Puertas, R.Rodrigo, A.Molina, and F.W.Taylor. A non-LTE radiative transfer model for infrared bands in the middle atmosphere. I. Theoretical basis and application to the CO_2 15 μm bands. *J.Atmos. Terr. Phys.*, Vol.48, No 8, pp. 729-748, 1986.

Lopez-Puertas M. et al., 1986b:

M.Lopez-Puertas, R.Rodrigo, J.J.Lopez-Moreno, and F.W.Taylor. A non-LTE radiative transfer model for infrared bands in the middle atmosphere. II. CO_2 (2.7 and 4.3 μm) and water vapor (6.3 μm) and N_2 (1) and O_2(1) vibrational levels. *J.Atmos. Terr. Phys.*, Vol.48, No 8, pp. 749-764,1986.

Lopez-Puertas M. and Taylor F.W., 1989:

Carbon dioxide 4.3-μm emission in the Earth's atmosphere: A comparison between NIMBUS 7 SAMS measurements and non-local thermodynamic equilibrium radiative transfer calculations. *J.Geoph. Res.*, Vol. 94, No D10, pp.13045-13068, September 20, 1989.

Lopez-Puertas M. et al., 1992:

M.Lopez-Puertas, M.A.Lopez-Valverde, C.P.Rinsland, and M.R.Gunson. Analysis of the upper atmosphere $CO_2(\nu_2)$ vibrational temperatures retrieved from ATMOS/Spacelab 3 observations. *J.Geoph. Res.*, Vol. 97, No D18, pp. 20469-20478, December 20, 1992.

Manuilova R.O. and Shved G.M., 1992:

The 4.8 and 9.6 μm O_3 band emissions in the middle atmosphere. *J.Atmos. Terr. Phys.*, Vol. 54, No 9, pp. 1149-1168, 1992.

Mlynczak M.G. and Drayson S.R., 1990a:

Calculation of infrared limb emission by ozone in the terrestrial middle atmosphere. 1.Source functions. *J.Geoph. Res.*, Vol. 95, pp. 16497-16511, 1990.

Mlynczak M.G. and Drayson S.R., 1990b:

Calculation of infrared limb emission by ozone in the terrestrial middle atmosphere. 2.Emission calculations *J.Geoph. Res.*, Vol. 95, pp. 16513-16521, 1990.

Oelhaf H. and Fischer H., 1989:

Relevance of upper atmosphere non-LTE effects to limb emission of stratospheric constituents. In: *"IRS'88: Current problems in atmospheric radiation"*, J.Lenoble and J.-P.Geleyn (Eds), A.Deepak Publishing, 1989.

Ogibalov V.P. et al., 1995:

V.P.Ogibalov, A.A.Kutepov, and G.M.Shved. Non-LTE in the CO_2 in the middle atmosphere. EGS XX General Assembly, Hamburg, Germany, 2-7 April, 1995.

Rothman L.S. et al., 1992:

Rothman L.S., Gamache R.R., Tipping R.H., Rinsland C.P., Smith M.A.H., D.Chris Benner, V.Malathy Devi, Flaud J.-M., Camy-Peyret C., Perrin A., Goldman A., Massie S.T., Brown L.R., Toth R.A. The HITRAN molecular database: editions of 1991 and 1992. *J.Quant. Spectrosc. Radiat. Transfer*, Vol. 48, No 5/6, pp. 469-507, 1992.

Smith D.R. and Ahmadjian M., 1993:

Observation of nitric oxide rovibrational band head emissions in the quiscent airglow during the CIRRIS-1A space shuttle experiment. *Geophysical Research Letters*, Vol. 20, No 23, pp. 2679-2682, December 14, 1993.

Timofeyev Yu.M. et al., 1986:

Yu.M.Timofeyev, V.V.Rozanov, A.V.Poberovsky, A.V.Polyakov. Multispectral measuring O_3 and NO_2 vertical profiles and aerosol extinction of atmospheric radiation. *Meteorology and Hydrology*, No 8, pp. 66-73, 1986.

Timofeyev Yu.M. et al., 1995:

Yu.M.Timofeyev, V.S.Kostsov, H.Grassl. Numerical investigations of the accuracy of the remote sensing of non-LTE atmosphere by space-borne spectral measurements of limb IR radiation: 15 μm CO_2 bands, 9.6 μm O_3 bands and 10 μm CO_2 laser bands. *Journal of Quantitative Spectroscopy and Radiative Transfer*, Vol. 53, No 6, pp. 613-632, 1995.

Wintersteiner P.P. et al., 1992:

P.P.Wintersteiner, R.H.Picard, R.D.Sharma, J.R.Winick, and R.A.Joseph. Line-by-line radiative excitation model for the non-equilibrium atmosphere: Application to CO_2 15-μm emission. *J.Geoph. Res.*, Vol. 97, No D16, pp. 18083-18117, November 20, 1992.